A Continuum Thermodynamics Formulation for Micro-magneto-mechanics with Applications to Ferromagnetic Shape Memory Alloys

Chad M. Landis
Department of Aerospace Engineering and Engineering Mechanics
The University of Texas at Austin
210 East 24th Street, C0600
Austin, TX 78712-0235
Phone: (512) 471-4273, Fax: (512) 471-5500
E-mail: landis@mail.utexas.edu

Abstract

A continuum thermodynamics formulation for micromagnetics coupled with mechanics is devised to model the evolution of magnetic domain and martensite twin structures in ferromagnetic shape memory alloys. The theory falls into the class of phase-field or diffuse-interface modeling approaches. In addition to the standard mechanical and magnetic balance laws, two sets of micro-forces and their associated balance laws are postulated; one set for the magnetization order parameter and one set for the martensite order parameter. Next, the second law of thermodynamics is analyzed to identify the appropriate material constitutive relationships. The proposed formulation does not constrain the magnitude of the magnetization to be constant, allowing for spontaneous magnetization changes associated with strain and temperature. The equations governing the evolution of the magnetization are shown to reduce to the commonly accepted Landau-Lifshitz-Gilbert equations for the case that the magnetization magnitude is constant. Furthermore, the analysis demonstrates that under certain limiting conditions, the equations governing the evolution of the martensite free strain are shown to be equivalent to a hyperelastic strain gradient theory. Finally, numerical solutions are presented to investigate the fundamental interactions between the magnetic domain wall and the martensite twin boundary in ferromagnetic shape memory alloys. These calculations determine under what conditions the magnetic domain wall and the martensite twin boundary can be dissociated, resulting in a limit to the actuating strength of the material.

Keywords: micromagnetics, magneto-mechanical coupling, domain wall structure, domain wall - twin boundary dissociation

1. Introduction

Ferromagnetic shape memory alloys (FSMAs) are materials with very strong magnetic and mechanical coupling. For example, in nickel-magnesium-gallium (NiMnGa) alloys

applied magnetic fields can cause actuation strains on the order of 6-10% (Tickle and James, 1999; Tickle, 2000; Murray *et al*., 2001; and Sozinov *et al*., 2002), while other magnetostrictive materials of interest like Terfenol and Galfenol can provide strains at not even one tenth of this level. The large strain in NiMnGa is due to the coupling between the mechanical twin structure and the magnetic domain structure (James and Wuttig, 1998; O'Handley *et al*., 2000; Kiefer and Lagoudas, 2005, and Ma and Li 2007a,b). Below the Curie temperature NiMnGa has a tetragonal crystal structure with the *c*-axis shorter than the *a*-axes. The material is also ferromagnetic with its easy axis of magnetization aligned with the *c*-axis. As in all martensitic and ferromagnetic materials, domain structures are formed that tend to minimize the energies associated with elastic and magnetic interactions, stray fields, and domain wall and twin boundary surface energies. When the magnetocrystalline anisotropy energy is high, the magnetic domain walls and martensite twin boundaries lie on top of one another and tend to move through the crystal in concert. Such cooperative defect motions furnish the material with the potential to deliver large actuating strains through the application of a magnetic field. However, these strains are significantly smaller in the presence of a blocking stress. Specifically, experimental investigations on NiMnGa materials have shown that practically no actuating strains exist even for large levels of applied magnetic field, if the material is under a 2-5 MPa compressive stress, Karaca *et al*. (2006). Hence, even though large stress-free strains can be obtained from FSMAs, these materials are not able to supply much actuation *energy* due to the relatively low blocking stress, Kiefer *et al*. (2007).

This paper presents a theoretical approach to describe magnetic domain walls, martensite twin boundaries, and their nonlinear interactions. The approach differs from "constrained" approaches (DeSimone and James 1997, 2002; Ma and Li, 2007a) where the evolution of energy minimizing laminate domain structures are studied, and the detailed structure and behavior of the domain walls is not considered. Instead, the theory falls into the class of "phase-field" or "diffuse interface" theories, wherein the material interfaces have a well-defined thickness, Chen (2002). The approach reduces to the accepted Landau-Lifshitz-Gilbert (LLG) equations for the micromagnetic response, and to the Landau-Ginzburg phase-field equations for the "microelastic" response. Unlike traditional methods for deriving the governing phase-field equations, which rely on energy minimization concepts, this paper applies a continuum thermodynamics approach. Specifically, the theory postulates the existence of micro-forces that are work conjugate to the martensite and magnetic order parameters, and associated balance laws for these micro-forces. Thereafter, the second law of thermodynamics is analyzed to obtain the appropriate constitutive equations and restrictions on the dissipation.

To apply the theory to a material class of interest, a material free energy is selected to mimic the behavior of ferromagnetic shape memory alloys. The governing micro-magneto-mechanical equations are solved to determine the magnetic domain wall and

martensite twin boundary structures. An analysis of the energetic forces that cause motion of these defects is also given. Finally, it is hypothesized that the mechanism for the low blocking stress levels in these materials is the dissociation of the martensite twin boundaries from the 90º magnetic domain walls. The model is used to predict several features of this behavior including the critical stress required to tear the martensite twin from the magnetic domain wall. The calculations are shown to predict blocking stress levels similar to those found experimentally.

2. Theory

Traditionally, the micromagnetics equations governing the evolution of domain configurations have been derived from a simple and physically justifiable set of assumptions (Landau and Lifshitz, 1935; Gilbert, 1956, 2004; and Brown, 1963). While this approach is certainly sound, it obscures the continuum physics distinction between fundamental balance laws, which are applicable to a wide range of materials, and the constitutive equations that are valid for a specific material (Fried and Gurtin, 1993, 1994; Gurtin, 1996). Here a small deformation non-equilibrium thermodynamics framework for ferromagnetic domain and martensite twin evolution is presented. The fundamental equations governing the magneto-mechanical fields under the assumption of small deformations and rotations are used as the starting point. Note that the small deformation assumption is prevalent throughout the micromagnetic modeling literature. The analysis of large deformations would introduce the concept of Maxwell stresses, which are here assumed to be higher order effects that can be neglected. Following previous micromagnetic modeling approaches, e.g. Zhang and Chen (2005a,b), the effects of large deformations will not be considered, but their incorporation within the theory is possible. It will also be assumed that the fields vary slowly in time with respect to any electromagnetic fluctuations in the material, yielding the quasi-static electromagnetic field approximation, but not necessarily with respect to the speed of sound, allowing for inertial effects to be considered within the general derivation. Under these assumptions, the balances of linear and angular momentum in any arbitrary volume V and its bounding surfaces S yield,

$$\sigma_{ji,j} + b_i = \rho \ddot{u}_i \quad \text{in} \quad V, \tag{2.1}$$

$$\sigma_{ij} = \sigma_{ji} \quad \text{in} \quad V, \tag{2.2}$$

$$\sigma_{ji} n_j = t_i \quad \text{on} \quad S. \tag{2.3}$$

Where σ_{ij} are the Cartesian components of the Cauchy stress, b_i the components of a body force per unit volume, ρ is the mass density, u_i the mechanical displacements, n_i

the components of a unit vector normal to a surface element, and t_i the tractions applied to a surface. Standard index notation is used with summation implied over repeated indices, the double overdot represents a second derivative with respect to time, and $,j$ represents partial differentiation with respect to the x_j coordinate direction. Under the assumptions of linear kinematics, the strain components ε_{ij} are related to the displacements as

$$\varepsilon_{ij} = \frac{1}{2}\left(u_{i,j} + u_{j,i}\right) \text{ in } V. \tag{2.4}$$

The magnetic field, H_i, magnetic induction, B_i, volume current density, J_i, surface current density, K_i, and the magnetic vector potential A_i, are governed by the quasi-static forms of Maxwell's equations. Specifically, in any arbitrary volume V (including a region of free space) and its bounding surface S,

$$B_{i,i} = 0 \quad \Rightarrow \quad B_i = \epsilon_{ijk} A_{k,j} \text{ in } V, \tag{2.5}$$

$$\epsilon_{ijk} H_{k,j} = J_i \text{ in } V, \tag{2.6}$$

$$\epsilon_{ijk} H_j n_k = K_i \text{ on } S. \tag{2.7}$$

Here ϵ_{ijk} is the permutation tensor such that $\epsilon_{ijk} = 1$ if ijk=123, 231, or 312, $\epsilon_{ijk} = -1$ if ijk=321, 132, or 213, and $\epsilon_{ijk} = 0$ for all other combinations of ijk. Within the theory of small deformation magnetostriction, Equations (2.1)-(2.7) represent the fundamental balance laws and kinematic relationships, and the constitutive laws required to close the loop on the equations relate the stress and magnetic field to the strain and magnetic induction. Such constitutive relationships can be derived from thermodynamic considerations using a material free energy that depends on the components of the strain and magnetic induction (Nye, 1957). However, within the micro-magneto-mechanical modeling approach derived here the free energy will also be required to depend on the magnetization and its gradient, and on the martensite free strain and its gradient. Note that the relationship between magnetic field, magnetic induction and material magnetization is given as

$$B_i = \mu_0\left(H_i + M_i\right) \text{ in } V. \tag{2.8}$$

Here μ_0 is the permittivity of free space. Given that the free energy will be allowed to depend on an additional independent variable M_i, we must now allow for a new system of "micro-forces" that are work conjugate to this configurational quantity. Following the work of Fried and Gurtin (1993, 1994, 1996), we introduce a micro-force tensor ξ_{ji} such that $\xi_{ji} n_j \dot{M}_i$ represents a power density expended across surfaces by neighboring configurations, an *internal* micro-force vector π_i such that $\pi_i \dot{M}_i$ is the power density expended by the material internally, e.g. in the ordering of spin within the lattice (this micro-force will account for dissipation in the material), and an external micro-force vector f_i such that $f_i \dot{M}_i$ is a power density expended on the material by external sources. In micromagnetics the fundamental balance law relates the magnetic torque to the rate of change of the angular momentum, Landau and Lifshitz (1935). In the present continuum framework, for an arbitrary volume of material, this angular momentum balance takes the following form,

$$\frac{1}{\mu_0}\left(\int_S \epsilon_{ijk} M_j \xi_{li} n_l \, dS + \int_V \epsilon_{ijk} M_j \pi_k \, dV + \int_V \epsilon_{ijk} M_j f_k \, dV\right) = \int_V \frac{1}{\gamma_0} \dot{M}_i \, dV \, . \tag{2.9}$$

Here, $\gamma_0 = -g \left| e \right| \mu_0 / (2m) = -2.214 \times 10^5 \text{ m/(A} \cdot \text{s)}$ is the gyromagnetic ratio for an electron spin, although within this phenomenological framework γ_0 can be used as a free parameter. In Equation (2.9), the left-hand side is the torque associated with the moment of the micro-forces and the magnetization, and the right-hand side is the rate of change of the angular momentum associated with the changes in the magnetization. Application of the divergence theorem to the first term, and recognizing that this balance law must hold for any arbitrary volume, yields the following point-wise balance law,

$$\epsilon_{kji} M_j \left(\xi_{li,l} + \pi_i + f_i\right) + \epsilon_{kji} M_{j,l} \xi_{li} = \frac{\mu_0}{\gamma_0} \dot{M}_k \, . \tag{2.10}$$

Equation (2.10) will be shown to lead to the Landau-Lifshitz-Gilbert equation of micromagnetics after the analysis of the second law of thermodynamics is performed. Taking the cross product of Equation (2.10) with the magnetization leads to,

$$M^2 \left(\xi_{li,l} + \pi_i + f_i\right) - M_i M_j \left(\xi_{lj,l} + \pi_j + f_j\right) + \epsilon_{ijk} \epsilon_{jrs} M_{r,l} \xi_{ls} M_k = \epsilon_{ijk} \frac{\mu_0}{\gamma_0} \dot{M}_j M_k \, . \tag{2.11}$$

Equation (2.11) gives no information on how the micro-forces affect the rate of change of the magnetization parallel to its direction, i.e. the change in its magnitude. Therefore, it will be assumed that the micro-forces in the direction of the magnetization are always in equilibrium. This assumption implies that the changes in magnetization magnitude occur such that a micro-force balance along the magnetization direction holds at every instant in time. Physically such changes in magnitude are not instantaneous. However, it is assumed that these changes occur on much shorter time scales than those associated with the rotation of the magnetization. Mathematically, this balance condition is stated as,

$$M_j \left(\xi_{lj,l} + \pi_j + f_j \right) = 0 . \tag{2.12}$$

Then, applying this assumption within Equation (2.11) yields the following equation for the micro-forces,

$$\xi_{li,l} + \pi_i + f_i = \epsilon_{ijk} \frac{\mu_0}{\gamma_0 M^2} \dot{M}_j M_k - \frac{\epsilon_{ijk}\epsilon_{jrs}}{M^2} M_{r,l} \xi_{ls} M_k . \tag{2.13}$$

Equation (2.13) is ultimately a continuum statement of the conservation of angular momentum associated with the electronic spin *and* the balance of micro-forces in the direction of the magnetization. This equation will eventually be used to develop finite element formulations for numerical solutions of the coupled magneto-mechanical equations.

In the literature on ferroelectric materials the use of the polarization vector as the sole order parameter is prevalent and leads to a reasonable description of domain wall structures and domain wall surface energies, Su and Landis (2007). However, we have found that the same assumption for ferromagnetic shape memory alloys, i.e. employing the magnetization as the sole order parameter, leads to a somewhat unrealistic domain wall structure and domain wall energy. The difficulty arises in the description of the strain, which in this case is quadratic in the magnetization. The strain change between different martensite variants in NiMnGa alloys can be in the range of 6%, and with elastic properties on the order of 100 GPa, this leads to stresses within the domain walls of about 6 GPa. This relatively large stress state results in "thinning" of the domain walls in order to compensate for this large strain energy and reduce the overall energy of the wall. Consequently, it is expected that a more realistic description of FSMAs would incorporate a second strain-like order parameter in order to describe the martensite twin boundaries. In this paper, a second rank tensor order parameter with components ε^0_{ij} is introduced, and is used to describe the possible martensite variants. This quantity is referred to as the *free-strain*, and it is distinct from the spontaneous strain since it is

not a constant valued tensor. Specifically, considering only spatially homogenous states, the spontaneous strain is defined to be the strain state at zero stress, zero micro-force and zero magnetic field. Whereas, the free-strain is the strain state at zero stress but not necessarily zero micro-force and magnetic field. Again, we introduce a system of micro-forces, $\zeta_{kji} n_k$ (surface), ϑ_{ji} (internal), and g_{ji} (external), that do work on changes in ε^0_{ij}. Additionally, a balance of these micro-forces is assumed such that

$$\int_S \zeta_{kji} n_k \, dS + \int_V \vartheta_{ji} \, dV + \int_V g_{ji} \, dV = 0, \tag{2.14}$$

which implies the point-wise balance,

$$\zeta_{kji,k} + \vartheta_{ji} + g_{ji} = 0. \tag{2.15}$$

To remain as general as possible, it is assumed that the Helmholtz free energy of the material (including the free space occupied by the material) takes the following form

$$\psi = \psi\left(\varepsilon_{ij}, B_i, M_i, M_{i,j}, \dot{M}_i, \varepsilon^0_{ij}, \varepsilon^0_{ij,k}, \dot{\varepsilon}^0_{ij}\right). \tag{2.16}$$

Note that temperature plays a key role in magnetic and martensitic phase transitions near the Curie point or austenite to martensite transition temperature. Near the Curie temperature, changes in the magnetization *magnitude* are particularly important. For spatially homogeneous isothermal behavior, the Helmholtz free energy remains the appropriate energy functional with the additional complication that the material parameters of the free energy are temperature dependent. Here we will deal only with constant temperature behavior below the two transition temperatures, but recognize that the extension to spatially homogeneous temperature dependent behavior can be readily included within the present framework simply by specifying the temperature at which the material properties must be evaluated at each instant in time. In contrast, the inclusion of spatially *inhomogeneous* temperature dependent behavior, and the associated thermal diffusion, requires an analysis of the second law of thermodynamics including such effects. In such cases the temperature and entropy must be introduced as additional field variables within the theory and the numerical treatment. In this paper, only constant temperature cases will be considered.

For the isothermal processes below the transition temperatures under consideration, the second law of thermodynamics is written as the Clausius-Duhem (dissipation) inequality as

$$\int_V \dot{\psi} dV + \tfrac{d}{dt}\int_V \tfrac{1}{2}\rho \dot{u}_i \dot{u}_i \, dV \le \int_V \left(b_i \dot{u}_i + J_i \dot{A}_i + f_i \dot{M}_i + g_{ji} \dot{\varepsilon}^0_{ij} \right) dV + \int_S \left(t_i \dot{u}_i + K_i \dot{A}_i + \xi_{ji} n_j \dot{M}_i + \zeta_{kji} n_k \dot{\varepsilon}^0_{ij} \right) dS \,. \tag{2.17}$$

The left-hand side of this inequality represents the rate of change of the stored plus kinetic energy of the material (or free space). The right-hand side represents the work rates due to externally applied mechanical forces, steady currents, and micro-forces. Note that the internal micro-forces π_i and ϑ_{ji} do not contribute to the external power. The difference between the right and left-hand sides of the equation is simply the dissipation, and the inequality specifies that the dissipation must be non-negative. Analysis of the rate of change of the kinetic energy and the application of the divergence theorem to the surface integrals yields,

$$\int_V \dot{\psi} dV \le \int_V [\underbrace{(\sigma_{ji,j} + b_i - \rho \ddot{u}_i)}_{0 \text{ by Eq. (2.1)}} \dot{u}_i + \underbrace{(\epsilon_{ijk} H_{j,k} + J_i)}_{0 \text{ by Eq. (2.6)}} \dot{A}_i + (\xi_{ji,j} + f_i)\dot{M}_i + (\zeta_{kji,k} + g_{ji})\dot{\varepsilon}^0_{ij}] dV + \int_V (\underbrace{\sigma_{ji} \dot{u}_{i,j}}_{\sigma_{ji}\dot{\varepsilon}_{ij}} + H_j \underbrace{\epsilon_{ijk} \dot{A}_{i,k}}_{\dot{B}_j} + \xi_{ji} \dot{M}_{i,j} + \zeta_{kji} \dot{\varepsilon}^0_{ij,k}) dV \,. \tag{2.18}$$

For an arbitrary volume, application of Equations (2.13) and (2.16) then give,

$$\left(\frac{\partial \psi}{\partial \varepsilon_{ij}} - \sigma_{ji} \right) \dot{\varepsilon}_{ij} + \left(\frac{\partial \psi}{\partial B_i} - H_i \right) \dot{B}_i + \left(\frac{\partial \psi}{\partial M_{i,j}} - \xi_{ji} \right) \dot{M}_{i,j} + \left(\frac{\partial \psi}{\partial \varepsilon^0_{ij,k}} - \zeta_{kji} \right) \dot{\varepsilon}^0_{ij,k} + \left(\frac{\partial \psi}{\partial M_i} + \pi_i + \frac{\epsilon_{ijk}\epsilon_{jrs}}{M^2} M_{r,l} \xi_{ls} M_k \right) \dot{M}_i + \left(\frac{\partial \psi}{\partial \varepsilon^0_{ij}} + \vartheta_{ji} \right) \dot{\varepsilon}^0_{ij} + \frac{\partial \psi}{\partial \dot{M}_i} \ddot{M}_i \dot{\varepsilon}^0_{ij} + \frac{\partial \psi}{\partial \dot{\varepsilon}^0_{ij}} \ddot{\varepsilon}^0_{ij} \le 0 \tag{2.19}$$

Note that the assumption implicit to Equation (2.16) is that the stress, magnetic field, micro-force tensors, and internal micro-forces are each allowed to depend on ε_{ij}, B_i, M_i, $M_{i,j}$, $\dot{M}_i$, ε^0_{ij}, $\varepsilon^0_{ij,k}$, and $\dot{\varepsilon}^0_{ij}$. The question that can be raised is why must the free energy be allowed to depend on $\dot{M}_i$ and $\dot{\varepsilon}^0_{ij}$. The answer is that since the internal micro-forces π_i and ϑ_{ji} must be allowed to depend on $\dot{M}_i$ and $\dot{\varepsilon}^0_{ij}$ (it will be demonstrated that these terms are responsible for the dissipation), then all of the thermodynamic forces could also have such dependence (this is the principle of *equipresence*, Coleman and Noll, 1963). It will be shown that the second law inequality ultimately allows only π_i and ϑ_{ji} to depend on $\dot{M}_i$ and $\dot{\varepsilon}^0_{ij}$ (see Equations (2.20) and (2.21a-d)). Following the procedure of Coleman and Noll (1963), it is assumed that for a given thermodynamic state,

arbitrary levels of $\dot{\varepsilon}_{ij}$, $\dot{B}_i$, $\dot{M}_i$, $\dot{M}_{i,j}$, $\ddot{M}_i$, $\dot{\varepsilon}^0_{ij}$, $\dot{\varepsilon}^0_{ij,k}$, and $\ddot{\varepsilon}^0_{ij}$ are admissible through the appropriate control of the external sources b_i, J_i, f_i, and g_{ji}. For example, consider the selection of a set of time rates of b_i, J_i, f_i, and g_{ji} such that $\dot{\varepsilon}_{ij}$, $\dot{B}_i$, $\dot{\varepsilon}^0_{ij}$, $\dot{\varepsilon}^0_{ij,k}$, $\dot{M}_i$, and $\dot{M}_{i,j}$ are arbitrary. Given that the first six terms of (2.19) are independent of $\ddot{M}_i$ and $\ddot{\varepsilon}^0_{ij}$ and the last two terms are linear in $\ddot{M}_i$ and $\ddot{\varepsilon}^0_{ij}$, it is always possible to find some admissible $\ddot{M}_i$ and $\ddot{\varepsilon}^0_{ij}$ that violates (2.19) unless,

$$\frac{\partial \psi}{\partial \dot{M}_i} = 0\,, \quad \frac{\partial \psi}{\partial \dot{\varepsilon}^0_{ij}} = 0 \quad \Rightarrow \quad \psi = \psi\left(\varepsilon_{ij}, B_i, M_i, M_{i,j}, \varepsilon^0_{ij}, \varepsilon^0_{ij,k}\right). \tag{2.20}$$

Similar arguments apply to the other configurational variables yielding the following constitutive relationships

$$\sigma_{ji} = \frac{\partial \psi}{\partial \varepsilon_{ij}}, \; H_i = \frac{\partial \psi}{\partial B_i}, \; \xi_{ji} = \frac{\partial \psi}{\partial M_{i,j}}, \; \text{and} \; \zeta_{kji} = \frac{\partial \psi}{\partial \varepsilon^0_{ij,k}}. \tag{2.21a-d}$$

Finally, after defining $p_i \equiv \dfrac{\partial \psi}{\partial M_i}$ and $q_{ji} \equiv \dfrac{\partial \psi}{\partial \varepsilon^0_{ij}}$, the internal micro-forces π_i and ϑ_{ji} must satisfy

$$\left(\pi_i + \frac{\epsilon_{ijk}\epsilon_{jrs}}{M^2} M_{r,l}\xi_{ls} M + p_i\right)\dot{M}_i + \left(\vartheta_{ji} + q_{ji}\right)\dot{\varepsilon}^0_{ij} \le 0$$

$$\Rightarrow \; \pi_i = -\frac{\epsilon_{ijk}\epsilon_{jrs}}{M^2} M_{r,l}\xi_{ls} M_k - p_i - \beta_{ij}\dot{M}_j - \omega_{ikl}\dot{\varepsilon}^0_{kl}, \quad \vartheta_{ij} = -q_{ij} - \varpi_{kij}\dot{M}_k - \kappa_{ijkl}\dot{\varepsilon}^0_{kl}\,. \tag{2.22}$$

such that $\beta_{ij}\dot{M}_i\dot{M}_j + \omega_{ikl}\dot{M}_i\dot{\varepsilon}^0_{kl} + \varpi_{kij}\dot{M}_k\dot{\varepsilon}^0_{ij} + \kappa_{ijkl}\dot{\varepsilon}^0_{ij}\dot{\varepsilon}^0_{kl} \ge 0$

If the existence of a dissipation potential $\Omega(\dot{\varepsilon}^0_{ij}, \dot{M}_i)$ is assumed, then the "viscosity" tensors can be derived as,

$$\beta_{ij} = \frac{\partial^2 \Omega}{\partial \dot{M}_i \partial \dot{M}_j}, \quad \omega_{kij} = \varpi_{kij} = \frac{\partial^2 \Omega}{\partial \dot{M}_k \partial \dot{\varepsilon}^0_{ij}}, \quad \text{and} \quad \kappa_{ijkl} = \frac{\partial^2 \Omega}{\partial \dot{\varepsilon}^0_{ij} \partial \dot{\varepsilon}^0_{kl}}. \tag{2.23}$$

The combined "viscosity" matrix is then guaranteed to be positive definite if the dissipation potential is convex.

Next, we demonstrate that the magnetic part of this theory is equivalent to the Landau-Lifshitz-Gilbert equations. If the "viscosity" tensor $\boldsymbol{\beta}$ is constant and the high temperature phase is cubic then $\beta_{ij} = \beta\delta_{ij}$ where $\beta \geq 0$, and δ_{ij} is the Kronecker delta. This is the simplest and most widely applied form for β_{ij}, and the scalar β is related to the parameter α in the Landau-Lifshitz-Gilbert equations. Substitution of Equations (2.21c) and (2.22) into the micro-force balance of Equation (2.13) yields a generalized form of the Landau-Lifshitz-Gilbert equations governing the evolution of the material magnetization in a magnetic material,

$$\left(\frac{\partial \psi}{\partial M_{i,j}}\right)_{,j} - \frac{\partial \psi}{\partial M_i} + f_i = \beta_{ij}\dot{M}_j + \frac{\mu_0}{\gamma_0 M^2}\epsilon_{ijk}\dot{M}_j M_k \quad \text{in} \quad V. \tag{2.24}$$

To demonstrate that this equation is equivalent to the Landau-Lifshitz-Gilbert equation, recognize that the effective magnetic field is

$$H_i^{eff} = \frac{1}{\mu_0}\left[\left(\frac{\partial \psi}{\partial M_{i,j}}\right)_{,j} - \frac{\partial \psi}{\partial M_i} + f_i\right]. \tag{2.25}$$

Then, taking the cross product of the magnetization with Equation (2.24), using $\beta_{ij} = \beta\delta_{ij}$, and rearranging terms yields,

$$\epsilon_{ijk}M_j\left(H_k^{eff} - \frac{\beta}{\mu_0}\dot{M}_k\right) = \frac{1}{\gamma_0 M^2}\epsilon_{ipj}M_p\epsilon_{jkl}\dot{M}_k M_l. \tag{2.26}$$

For most magnetic materials the magnetization magnitude is nearly constant at a given temperature. The Landau-Lifshitz-Gilbert equation is only able to analyze situations where the magnetization magnitude does not change at a given point (although this magnitude may differ at two distinct points). In such cases, the magnetization magnitude is equal to the spontaneous magnetization M_s (which is perhaps spatially inhomogeneous). In order to represent this situation within the present theory a term is needed in the free energy of the form,

$$\psi_{\text{constraint}} = \frac{\mu_0\left(1+\chi_m\right)}{2\chi_m}(M - M_s)^2. \tag{2.27}$$

The rationale for this term is discussed in greater detail after Equation (2.36). For the present purpose, we are interested in the limit as $\chi_m \to 0$. In this case, the only solution for the magnetization magnitude that satisfies Equation (2.12) is $M = M_s$. For such a constant magnetization magnitude, Equation (2.26) simplifies to,

$$\epsilon_{ijk} M_j \left(H_k^{eff} - \frac{\beta}{\mu_0} \dot{M}_k \right) = \frac{1}{\gamma_0} \dot{M}_i . \tag{2.28}$$

Equation (2.28) is the Landau-Lifshitz-Gilbert equation for micromagnetics, Gilbert (2004). The relationships between β and Gilbert's damping parameter η, and the more commonly used α (Kronmüller and Fähnle, 2003), are $\beta = \mu_0 \eta = \mu_0 \alpha / \left(\gamma_0 M_s \right)$. The primary differences between the present derivation of Equation (2.28) and the historical approach is that a set of energetic micro-forces is postulated which are work-conjugate to the magnetization, and the second law of thermodynamics is applied to constrain the free energy Eq. (2.20), identify the constitutive relationships of Eqs. (2.21a-d), and propose the general form for the internal material dissipation Eq. (2.22). The present framework is not restricted to cases where the magnitude of the magnetization is constant, and can be readily extended to spatially homogeneous temperature dependent behavior. However, when the constraint of a constant magnetization magnitude is enforced, the present approach reduces to the Landau-Lifshitz-Gilbert equation.

It is important to note that the free energy introduced in Equation (2.16) and further constrained in (2.20) includes both the energy stored in the material and the energy stored in the free space occupied by the material. This distinction becomes important when comparing this approach to others that separate the energy in the material from that stored in the stray fields. Specifically, in the present framework, the free energy must be decomposed into the free energy of the material and that of the free space such that,

$$\psi \left(\varepsilon_{ij}, B_i, M_i, M_{i,j}, \varepsilon_{ij}^0, \varepsilon_{ij,k}^0 \right) = \bar{\psi} \left(\varepsilon_{ij}, M_i, M_{i,j}, \varepsilon_{ij}^0, \varepsilon_{ij,k}^0 \right) + \frac{1}{2\mu_0} B_i B_i - M_i B_i . \tag{2.29}$$

Furthermore, for problems where the magnetic fields permeate into the vacuum (e.g. non-infinite material regions), then $\bar{\psi} = 0$ and $M_i = 0$ in regions of free space.

In order to generate numerical solutions to Equations (2.1)-(2.24) on arbitrary domains, the following principal of virtual work based on the mechanical displacements, the order parameters, and a scalar magnetic potential can be applied to derive finite element equations,

$$\begin{aligned}
&\int_V \beta_{ij}\dot{M}_j\,\delta M_i\,dV + \int_V \omega_{ikl}\dot{\varepsilon}^0_{kl}\,\delta M_i\,dV + \int_V \varpi_{kij}\dot{M}_k\,\delta\varepsilon^0_{ij}\,dV + \int_V \kappa_{ijkl}\dot{\varepsilon}^0_{kl}\,\delta\varepsilon^0_{ij}\,dV \\
&+\int_V \tfrac{1}{\gamma_0 M_s^2}\epsilon_{ijk}\dot{M}_j M_k \delta M_i dV + \int_V \rho\ddot{u}_i\,\delta u_i\,dV + \\
&+\int_V \sigma_{ji}\delta\varepsilon_{ij} - B_i\delta H_i + p_i\delta M_i + \xi_{ji}\delta M_{i,j} + q_{ji}\delta\varepsilon^0_{ij} + \zeta_{kji}\delta\varepsilon^0_{ij,k}dV \\
&= \int_V b_i\delta u_i + f_i\delta M_i + g_{ji}\delta\varepsilon^0_{ij}dV + \int_S t_i\delta u_i - B_n\delta\phi + \xi_{ji}n_j\delta M_i + \zeta_{kji}n_k\delta\varepsilon^0_{ij}dS
\end{aligned} \quad . \tag{2.30}$$

The magnetic field is derived from the scalar magnetic potential ϕ and a vector current potential φ_i as,

$$H_i = -\phi_{,i} + \varphi_i \tag{2.31}$$

with

$$J_i = \epsilon_{ijk}\varphi_{k,j} \tag{2.32}$$

and

$$B_n = B_i n_i \text{ on the surface } S. \tag{2.33}$$

For a given boundary value problem the current J_i is specified and the vector current potential can be chosen in any way that satisfies (2.32). Either the normal component of the magnetic induction or the magnetic potential must be specified at all points on the bounding surface. For problems where the permeation of the magnetic fields into the surrounding free space is important, a Dirichlet to Neumann map can be applied on the boundary, Givoli and Keller (1989).

For this form of the principal of virtual work the magnetic enthalpy defined as $h = \psi - B_i H_i$ is the required free energy functional and is dependent on H_i instead of B_i. The constitutive relations analogous to those in (2.21a-d) then become

$$\sigma_{ji} = \frac{\partial h}{\partial\varepsilon_{ij}},\ B_i = -\frac{\partial h}{\partial H_i},\ \xi_{ji} = \frac{\partial h}{\partial M_{i,j}},\ \zeta_{kji} = \frac{\partial h}{\partial\varepsilon^0_{ij,k}},\ g_{ji} = \frac{\partial h}{\partial\varepsilon^0_{ij}} \text{ and } p_i = \frac{\partial h}{\partial M_i}. \tag{2.34}$$

Another form of the principal of virtual work utilizing the vector potential A_i can also be established, but will introduce more degrees of freedom per node into the finite element formulation. This form of the principal of virtual work is,

$$\begin{aligned}
&\int_V \beta_{ij}\dot{M}_j\,\delta M_i\,dV + \int_V \omega_{ikl}\dot{\varepsilon}^0_{kl}\,\delta M_i\,dV + \int_V \varpi_{kij}\dot{M}_k\,\delta\varepsilon^0_{ij}\,dV + \int_V \kappa_{ijkl}\dot{\varepsilon}^0_{kl}\,\delta\varepsilon^0_{ij}\,dV \\
&+ \int_V \tfrac{1}{\gamma_0 M_s^2}\epsilon_{ijk}\dot{M}_j M_k \delta M_i dV + \int_V \rho\ddot{u}_i\,\delta u_i\,dV + \\
&+ \int_V \sigma_{ji}\delta\varepsilon_{ij} + H_i\delta B_i + p_i\delta M_i + \xi_{ji}\delta M_{i,j} + q_{ji}\delta\varepsilon^0_{ij} + \zeta_{kji}\delta\varepsilon^0_{ij,k}dV \\
&= \int_V b_i\delta u_i + J_i\delta A_i + f_i\delta M_i + g_{ji}\delta\varepsilon^0_{ij}dV + \int_S t_i\delta u_i + K_i\delta A_i + \xi_{ji}n_j\delta M_i + \zeta_{kji}n_k\delta\varepsilon^0_{ij}dS
\end{aligned} \quad . \tag{2.35}$$

Next, the material free energy is specified. Ultimately, the goal is to apply this model to ferromagnetic shape memory alloys (FSMAs) with strong magnetic and mechanical coupling. Note that arbitrarily general and complex forms for the free energy can be introduced into the theoretical framework, however here the following relatively simple form for the free energy for tetragonal martensite is introduced,

$$\begin{aligned}
\psi &= \tfrac{1}{2}a_0^M M_{i,j}M_{i,j} + \tfrac{1}{2}a_0^\varepsilon \varepsilon^0_{ij,k}\varepsilon^0_{ij,k} \\
&+ \frac{K_1}{\varepsilon_0 M_s^2}\left[\left(\varepsilon^0_{11} + \varepsilon_0/2\right)\left(M_2^2 + M_3^2\right) + \left(\varepsilon^0_{22} + \varepsilon_0/2\right)\left(M_1^2 + M_3^2\right) + \left(\varepsilon^0_{33} + \varepsilon_0/2\right)\left(M_1^2 + M_2^2\right)\right] \\
&- \frac{2}{3}\frac{K_1}{\varepsilon_0^2}\left[\varepsilon^0_{11}\varepsilon^0_{22} + \varepsilon^0_{11}\varepsilon^0_{33} + \varepsilon^0_{22}\varepsilon^0_{33} + \varepsilon_0\left(\varepsilon^0_{11} + \varepsilon^0_{22} + \varepsilon^0_{33}\right)\right] \\
&+ \frac{K_2}{\varepsilon_0 M_s^2}\left[\left(\varepsilon^0_{12} + \varepsilon^0_{21}\right)M_1M_2 + \left(\varepsilon^0_{13} + \varepsilon^0_{31}\right)M_1M_3 + \left(\varepsilon^0_{23} + \varepsilon^0_{32}\right)M_2M_3\right] \\
&+ \frac{b_1}{2}\left(\varepsilon^0_{kk}\right)^2 + \frac{b_2}{3}\left[\left(e^0_{11}\right)^3 + \left(e^0_{22}\right)^3 + \left(e^0_{33}\right)^3\right] + \frac{b_3}{4}\left[\left(e^0_{11}\right)^4 + \left(e^0_{22}\right)^4 + \left(e^0_{33}\right)^4\right] \\
&+ \frac{b_4}{2}\left[\left(\varepsilon^0_{12}\right)^2 + \left(\varepsilon^0_{21}\right)^2 + \left(\varepsilon^0_{13}\right)^2 + \left(\varepsilon^0_{31}\right)^2 + \left(\varepsilon^0_{23}\right)^2 + \left(\varepsilon^0_{32}\right)^2\right] \\
&+ \tfrac{1}{2}\bar{c}_{ijkl}\left(\varepsilon_{ij} - \varepsilon^0_{ij}\right)\left(\varepsilon_{kl} - \varepsilon^0_{kl}\right) \\
&+ \frac{1}{2\mu_0}B_iB_i - M_iB_i + \frac{\mu_0\left(1 + \chi_m\right)}{2\chi_m}\left(M - M_s\right)^2 + \mu_0 M_s M
\end{aligned} \tag{2.36}$$

$$e^0_{ij} = \varepsilon^0_{ij} - \tfrac{1}{3}\varepsilon^0_{kk}\delta_{ij} \tag{2.37}$$

$$M = \sqrt{M_iM_i}\ . \tag{2.38}$$

First note that the structure of the free energy must contain the symmetry of the high temperature material phase, which for most FMSAs of interest is cubic. The first terms of the free energy are the exchange energies, which penalize large gradients of magnetization and free-strain, and give magnetic domain walls and martensite twin boundaries thickness and energy within the theory. The next three lines represent the magnetocrystalline anisotropy energy that creates energy wells at the preferred orientations for the magnetization. For many FSMAs with tetragonal structure the *c*-axis is shorter than the *a*-axes and the magnetization is in a low energy state when it is aligned with the *c*-axis. The fifth and sixth lines contain the energy landscape associated with the free-strain. These terms have energy wells located at the stress-free spontaneous strain states of the martensite phase, and the form of the spontaneous strain effectively defines the symmetry of the low temperature martensite phase. Note that e_{ij}^0 is the deviatoric part of the free-strain as defined in Equation (2.37). The seventh line of the free energy couples the free-strain to the total strain. It is important to note that the $\bar{c}_{ijkl}$ tensor is *not* the elastic stiffness tensor that would be measured in the laboratory. This is the elastic stiffness measured at constant free-strain ε_{ij}^0. What is measured in the lab is the stiffness at constant micro-force q_{ij}. Hence, the measured stiffness contains contributions from both $\bar{c}_{ijkl}$ and the curvature of the energy wells at the stress-free spontaneous strain state. Further analysis of these elastic properties will be discussed shortly. The last two terms in Equation (2.36) represent the energy associated with changes in the magnitude of the magnetization. The vast majority of the micromagnetics literature assumes the constraint $M = M_s$, where M_s is the spontaneous magnetization. In this work it is assumed that there exists some paramagnetic or diamagnetic (depending on if $\chi_m > 0$ or $\chi_m < 0$) behavior of the material about the spontaneously magnetized state characterized by the magnetic susceptibility χ_m such that $(M - M_s)M_i / M = \chi_m H_i$. The constraint of $M = M_s$ is then enforced in the limit that $\chi_m \to 0$. For $|\chi_m| \ll 1$, there is a significant energy penalty for magnetization states with magnitudes far from M_s. Hence, this term is a realistic representation that the magnetization is "practically equal to the saturation moment" as quoted from Landau and Lifshitz (1935). An isotropic form for the paramagnetic/diamagnetic response of the magnetization about the spontaneous state has been assumed, but more general anisotropic forms can also be used. One of the benefits of this term, aside from the fact that it should exist on physical grounds, is that no special techniques are required to enforce the constraint of $M = M_s$ in the numerical solutions to the governing equations. On the other hand, this term is detrimental to formulating *analytical* solutions, and it is simpler to use the $M = M_s$ constraint when analytical solutions can be obtained.

At this point it is worth discussing the similarities and differences between the descriptions of the martensite order parameter in this work and previous approaches, e.g. Jin *et al*. (2001) and Wang *et al*. (2004). In this work we follow Zhang and Chen (2005a) and implement a second rank tensor to describe the free-strain and further assume that this tensor is symmetric. Unlike Zhang and Chen, this work allows for the shear components of the free strain to exist, and hence this description provides six independent components to describe the free-strain of the material. We argue that no more independent variables should be required to describe the stress-free spontaneous strain state of any given material variant. Previous approaches, Jin *et al*. (2001) and Wang *et al*. (2004), have relied on a set of scalar order parameters coupled with constant second rank tensors to describe the free-strain. The number of scalar order parameters required to represent an austenite to tetragonal martensite transition would be four for such a description as opposed to six. However, for more complex structures of the low symmetry phase, or for multiple low symmetry phases, the scalar approach can easily exceed six order parameter fields. For the case where the number of scalar order parameters is less than six, such a treatment can be viewed as a constrained version of the present theory, in other words certain free-strain states are unattainable. However, if the free strain provides the fundamental description of the material state, then when more than six order parameters are implemented, special care must be exercised to ensure that different sets of order parameters, yielding the same free-strain, result in the same free energy. Effectively this implies that a maximum of six scalar order parameters can be considered as independent, and in this case the general form of the present theory would be recovered (the specific form of (2.36) would not necessarily apply).

As mentioned previously it is important to note, in both this work and in the prior approaches referenced above, that the tensor $\bar{c}_{ijkl}$ is not the elastic stiffness that would be measured in the laboratory. This is more readily recognized if an uncoupled, purely mechanical theory is considered, wherein the stress or strain would be given as,

$$\sigma_{ij} = \bar{c}_{ijkl}\left(\varepsilon_{kl} - \varepsilon^0_{kl}\right) \quad \Rightarrow \quad \varepsilon_{ij} = \bar{s}_{ijkl}\sigma_{kl} + \varepsilon^0_{kl}\,. \tag{2.39}$$

The second of Equations (2.39) reveals the issue. If a stress is applied and the free-strain were to remain constant, then $\bar{s}_{ijkl}$ would be the compliance that is measured. However, the physically relevant condition is not to fix the free strain, but rather to keep the micro-force fixed, i.e. $q_{ji} \equiv \partial\psi \big/ \partial\varepsilon^0_{ij} = 0$. Under the zero micro-force conditions the applied stress *does* cause a change in free-strain, and thus an additional component to the total strain change, leading to a difference between $\bar{s}_{ijkl}$ and the measured

compliance. If we define $f(\varepsilon_{ij}^0)$ to be the energy landscape associated with the free strain (e.g. lines 5 and 6 of (2.36)), and the measured elastic stiffness to be the derivative of the stress with respect to the strain at fixed/zero micro-force, then it can be shown that the measured elastic stiffness is,

$$c_{ijkl} = \left.\frac{\partial \sigma_{ij}}{\partial \varepsilon_{kl}}\right|_{q_{ij}=0} = f_{ijmn}\left(f_{mnpq} + \bar{c}_{mnpq}\right)^{-1}\bar{c}_{pqkl} \tag{2.40}$$

where

$$f_{ijkl} \equiv \left.\frac{\partial^2 f}{\partial \varepsilon_{ij}^0 \partial \varepsilon_{kl}^0}\right|_{\varepsilon_{pq}^0 = \varepsilon_{pq}^s} . \tag{2.41}$$

Note that all of these properties are actually the tangent properties at the spontaneous, stress-free and micro-force-free, strain states ε_{pq}^s. Also note that f_{ijkl} represents the curvature of the energy wells at the spontaneous strain states. Equation (2.40) indicates that $\bar{c}_{ijkl}$ is only a good approximation to the measured elastic stiffness if the curvature of the energy wells is very large. In this case, the free-strain is not able to depart significantly from the spontaneous strain and is effectively constant in the absence of switching/transformation. Perhaps a more physically appealing limit is the case where $\bar{c}_{ijkl}$ is very large. In this case, the energy landscape not only dictates the structure of the low symmetry phases and the energy barriers between them, but the elastic properties are also given by the curvature of the energy wells. Furthermore, in the limit as the principal values of $\bar{c}_{ijkl}$ go to infinity, the present phase field theory becomes a hyperelastic strain gradient theory. This is demonstrated using the uncoupled, purely mechanical version of the theory. Take the free energy to be of the following form,

$$\psi = g\left(\varepsilon_{ij,k}^0\right) + f\left(\varepsilon_{ij}^0\right) + \tfrac{1}{2}\bar{c}_{ijkl}\left(\varepsilon_{ij} - \varepsilon_{ij}^0\right)\left(\varepsilon_{kl} - \varepsilon_{kl}^0\right). \tag{2.42}$$

Since

$$\sigma_{ij} = \frac{\partial \psi}{\partial \varepsilon_{ij}} = \bar{c}_{ijkl}\left(\varepsilon_{kl} - \varepsilon_{kl}^0\right), \tag{2.43}$$

the stresses can only remain finite if $\varepsilon_{ij} \to \varepsilon_{ij}^0$ in the limit as the principal values of $\bar{c}_{ijkl}$ go to infinity. Next, the micro-force balance of (2.15) becomes

$$\left(\frac{\partial g}{\partial \varepsilon^0_{ij,k}}\right)_{,k} - \frac{\partial f}{\partial \varepsilon^0_{ij}} + \sigma_{ji} - \kappa_{ijkl}\dot{\varepsilon}^0_{kl} = 0$$
$$\Rightarrow \sigma_{ji} = \frac{\partial f}{\partial \varepsilon^0_{ij}} - \left(\frac{\partial g}{\partial \varepsilon^0_{ij,k}}\right)_{,k} + \kappa_{ijkl}\dot{\varepsilon}^0_{kl} \quad . \tag{2.44}$$

Finally, Equation (2.1) becomes

$$\left(\frac{\partial f}{\partial \varepsilon^0_{ij}}\right)_{,j} - \left(\frac{\partial g}{\partial \varepsilon^0_{ij,k}}\right)_{,kj} + \left(\kappa_{ijkl}\dot{\varepsilon}^0_{kl}\right)_{,j} + b_i = \rho\ddot{u}_i \, . \tag{2.45}$$

Using $\varepsilon_{ij} = \varepsilon^0_{ij}$, Equation (2.45) is equivalent to the linear momentum balance in a strain gradient theory for a material with free energy $\psi = g\left(\varepsilon_{ij,k}\right) + f\left(\varepsilon_{ij}\right)$ and viscous stresses $\kappa_{ijkl}\dot{\varepsilon}^0_{kl}$. Hence, one approach within this theory is to construct $f(\varepsilon^0_{ij})$ to represent all of the martensite properties, including the elasticity, and then use large values of $\overline{c}_{ijkl}$ to enforce the constraint $\varepsilon_{ij} = \varepsilon^0_{ij}$. In this sense, $\overline{c}_{ijkl}$ can be viewed as the mechanical analog of χ_m. The results presented in the next section follow exactly this approach.

3. Planar Domain Wall Solutions

In this section the analysis of straight domain walls in the *y*-*z* plane moving at constant velocity *v* in the *x*-direction is presented. Generalized plane strain is assumed such that $\varepsilon_{xz} = \varepsilon_{yz} = 0$ and ε_{zz} is uniform. In a coordinate system that is moving along with the domain wall at constant velocity *v*, symmetry considerations dictate that the solutions for the components of stress, strain, magnetic field, magnetic induction, magnetization, free strain and all micro-forces are functions of *x* only. Given these constraints, the compatibility of strains implied by Equation (2.4) yields

$$\varepsilon_{yy} = c_0 x + \varepsilon^0_{yy} \, . \tag{3.1}$$

With no free current J_i, Maxwell's laws governing the quasi-static magnetic induction and magnetic field distributions, Equations (2.5) and (2.6), imply that

$$\frac{dB_x}{dx} = 0 \quad \Rightarrow \quad B_x = B^0_x, \tag{3.2}$$

$$\frac{dH_y}{dx} = 0 \quad \Rightarrow \quad H_y = H_y^0, \tag{3.3}$$

$$\frac{dH_z}{dx} = 0 \quad \Rightarrow \quad H_z = H_z^0. \tag{3.4}$$

The parameters ε_{yy}^0, B_x^0, H_y^0 and H_z^0 are the constant axial strain, magnetic induction and magnetic field in the associated directions. The constant c_0 arises if the domain wall is curved due to the deformation. Here only cases where the wall remains straight after the deformation will be considered and hence c_0 is taken to be zero. Then, the fact that $\varepsilon_{xx} = \varepsilon_{xx}(x)$ implies that $u_{x,yx} = \varepsilon_{xx,y} = 0$, and the momentum balance of Equation (2.1), yields

$$\frac{d}{dx}\left(\sigma_{xx} - \rho v^2 \varepsilon_{xx}\right) = 0 \quad \Rightarrow \quad \sigma_{xx} = \rho v^2 \varepsilon_{xx} + \sigma_{xx}^0, \tag{3.5}$$

$$\frac{d}{dx}\left(\sigma_{xy} - 2\rho v^2 \varepsilon_{xy}\right) = 0 \quad \Rightarrow \quad \sigma_{xy} = 2\rho v^2 \varepsilon_{xy} + \sigma_{xy}^0, \tag{3.6}$$

$$\frac{d}{dx}\left(\sigma_{xz} - 2\rho v^2 \varepsilon_{xz}\right) = 0 \quad \Rightarrow \quad \sigma_{xz} = 2\rho v^2 \varepsilon_{xz} + \sigma_{xz}^0, \tag{3.7}$$

where σ_{xx}^0, σ_{xy}^0, and σ_{xz}^0 are constants. Finally, the micro-force balances of Equations (2.24) become

$$\frac{d\xi_{xi}}{dx} - p_i = -v\left(\beta_{ij}\frac{dM_j}{dx} + \omega_{ikl}\frac{d\varepsilon_{kl}^0}{dx} + \epsilon_{ijk}\frac{\mu_0}{\gamma_0 M^2}\frac{dM_j}{dx}M_k\right), \tag{3.8}$$

$$\frac{d\zeta_{xij}}{dx} - q_{ij} = -v\left(\kappa_{ijkl}\frac{d\varepsilon_{kl}^0}{dx} + \varpi_{kij}\frac{dM_k}{dx}\right). \tag{3.9}$$

Here the indices take on *x*, *y* or *z* values and repeated indices imply summation over *x*, *y* and *z*. The solutions to Equations (3.1)-(3.9) are subject to the boundary conditions $\sigma_{xx}(\infty) = \sigma_{xx}^+$, $\sigma_{xx}(-\infty) = \sigma_{xx}^-$, $\sigma_{xy}(\infty) = \sigma_{xy}^+$, $\sigma_{xy}(-\infty) = \sigma_{xy}^-$, $\sigma_{xz}(\infty) = \sigma_{xz}^+$, $\sigma_{xz}(-\infty) = \sigma_{xz}^-$, $B_x(\pm\infty) = B_x^0$, $p_i(\pm\infty) = 0$, and $q_{ij}(\pm\infty) = 0$. Along with these

boundary conditions the governing equations can be solved for the magnetomechanical structure of planar domain walls. Prior to presenting such results, an expression for the Eshelby driving traction on a magnetomechanical domain wall following the procedure of Fried and Gurtin (1994) is derived.

Sharp interface theories of domain wall dynamics require a kinetic law that describes the normal velocity of points along the interface. Such kinetic laws usually relate the normal velocity to the jump in the Eshelby energy-momentum tensor across the wall. The following derivation provides this relationship based on the present micro-magneto-mechanical theory. First, multiply Equations (3.2) and (3.5)-(3.9) by $-H_x$, ε_{xx}, $2\varepsilon_{xy}$, $2\varepsilon_{xz}$, $M_{i,x}$ and $\varepsilon^0_{ij,x}$ respectively. Then, once again defining the magnetic enthalpy as $h = \psi - H_i B_i$, the sum of these equations can be rearranged as follows,

$$\begin{aligned}&\frac{d}{dx}\Big(\xi_{xi}M_{i,x} + \zeta_{xji}\varepsilon^0_{ij,x} + \sigma_{xx}\varepsilon_{xx} + 2\sigma_{xy}\varepsilon_{xy} + 2\sigma_{xz}\varepsilon_{xz} \\ &\qquad - \tfrac{1}{2}\rho v^2\varepsilon^2_{xx} - 2\rho v^2\varepsilon^2_{xy} - 2\rho v^2\varepsilon^2_{xz} - H_x B_x - h\Big) \\ &= -v\Big(\beta_{ij}M_{i,x}M_{j,x} + \omega_{kij}M_{k,x}\varepsilon^0_{ij,x} + \varpi_{kij}M_{k,x}\varepsilon^0_{ij,x} + \kappa_{ijkl}\varepsilon^0_{ij,x}\varepsilon^0_{kl,x}\Big)\end{aligned} \quad . \tag{3.10}$$

After defining $\llbracket a \rrbracket = a(\infty) - a(-\infty)$ and $\langle a \rangle = \big[a(\infty) + a(-\infty)\big]/2$, and applying the identity $\llbracket ab \rrbracket = \langle a \rangle \llbracket b \rrbracket + \langle b \rangle \llbracket a \rrbracket$, the integral of Equation (3.10) from $x = -\infty$ to $x = \infty$ can be shown to yield,

$$f \equiv \llbracket h \rrbracket - \langle \sigma_{xx} \rangle \llbracket \varepsilon_{xx} \rrbracket - 2\langle \sigma_{xy} \rangle \llbracket \varepsilon_{xy} \rrbracket - 2\langle \sigma_{xz} \rangle \llbracket \varepsilon_{xz} \rrbracket + \langle B_x \rangle \llbracket H_x \rrbracket = \frac{1}{\mu} v \,, \tag{3.11}$$

where the Eshelby driving traction f is defined within Equation (3.11) and the domain wall mobility μ is defined as

$$\frac{1}{\mu} = \int_{-\infty}^{\infty} \Big(\beta_{ij}M_{i,x}M_{j,x} + \omega_{kij}M_{k,x}\varepsilon^0_{ij,x} + \varpi_{kij}M_{k,x}\varepsilon^0_{ij,x} + \kappa_{ijkl}\varepsilon^0_{ij,x}\varepsilon^0_{kl,x}\Big) dx \tag{3.12}$$

The left-hand side of Equation (3.11) is the jump in Eshelby's energy-momentum tensor, Eshelby (1970), across a flat planar domain wall moving in the x-direction. While solutions for moving domain walls are of interest (e.g. Thiele, 1974), in the following section only numerical results for zero velocity solutions to Equations (3.1)-(3.9) are presented.

The first set of results are shown in order to substantiate the claim that a material description that perfectly couples the martensite twin boundaries to the magnetic domain walls, similar to what is done for ferroelectrics, leads to an unrealistically thin (or high energy) domain wall structure. For such perfectly coupled cases the free strain is not an independent variable, and is determined directly from the magnetization as

$$\varepsilon_{ij}^{0} = \lambda_{ijkl} m_k m_l \,. \tag{3.13}$$

The reduced form of the free energy is then

$$\begin{aligned} \psi_{reduced} = {} & \tfrac{1}{2} a_0^M M_{i,j} M_{i,j} \\ & + \frac{k_{ijkl}}{M_s^4} M_i M_j M_k M_l + \frac{\bar{k}_{ijklpq}}{M_s^6} M_i M_j M_k M_l M_p M_q \\ & + \tfrac{1}{2} \bar{\bar{c}}_{ijkl} \left(\varepsilon_{ij} - \varepsilon_{ij}^{0}\right)\left(\varepsilon_{kl} - \varepsilon_{kl}^{0}\right) \\ & + \frac{1}{2\mu_0} B_i B_i - M_i B_i + \frac{\mu_0 \left(1 + \chi_m\right)}{2\chi_m}\left(M - M_s\right)^2 + \mu_0 M_s M \end{aligned} \tag{3.14}$$

$$\text{where } \bar{\bar{c}}_{ijkl} = \tilde{c}_{ijkl} + f_{ijklpq} \frac{M_p M_q}{M_s^2} \tag{3.15}$$

This constrained description of the free strain and the associated free energy will be referred to as the *perfectly coupled theory*. In other words, the free strain is perfectly/rigidly coupled to the magnetization. The set of material coefficients associated with Equations (2.36) and (3.14) is chosen to mimic the behavior of NiMnGa. The specific values for these coefficients are given in the Appendix. It is important to note that both the perfectly coupled and the general free energy descriptions yield the same (similar when the $\boldsymbol{f}$ tensor is zero) incremental magneto-mechanical response about the spontaneously magnetized state.

Figures 1-3 plot the magnetization, stress and strain profiles within a 180º Bloch wall (magnetization rotates within the plane of the wall), a 180º Néel wall (magnetization rotates out of the plane of the wall), and a 90º domain wall/twin boundary as predicted for both the perfectly coupled theory and the general theory in a bulk crystal. Thin films have not been studied in this work, but a recent review of analytical models that predict how thin film geometries affect the structure of magnetic domain walls can be found in DeSimone et al. (2006). For the perfectly coupled theory the coefficients of the $\boldsymbol{f}$ tensor have been set to zero to obtain more reasonable results. Inclusion of these coefficients makes the walls predicted by the perfectly coupled theory even thinner, and

the stresses within the walls even higher. In general, the additional energy associated with the magneto-mechanical coupling tends to thin the magnetic domain walls and the martensite twin boundaries. In fact, the perfectly coupled theory takes this coupling to the extreme and generates very thin walls.

All strain values are normalized by the magnitude of the spontaneous strain $\left|\varepsilon_0\right|$. Note that the *c*-axis is shorter than the *a*-axes in NiMnGa, so the spontaneous strain ε_0 is less than zero for this material. Two different stress normalizations can be used, σ_0 is defined such that $\sigma_0\left|\varepsilon_0\right|$ is the depth of the energy wells at the spontaneous strain states associated with the free energy of Equation (2.36), and $\sigma_M = K_1 \big/ \left|\varepsilon_0\right|$ is a characteristic stress that can be used for either the perfectly coupled or more general free energy description. Two length scale normalizations will be used,

$$l_\varepsilon = \sqrt{\frac{a_0^\varepsilon \left|\varepsilon_0\right|}{\sigma_0}} \tag{3.16}$$

and

$$l_M = \sqrt{\frac{a_0^M M_s^2}{K_1}}\,. \tag{3.17}$$

Again, this second length scale can be used with either free energy description. The domain wall and twin boundary thicknesses h_M and h_ε from any given calculation will be defined as,

$$h_M = \frac{M_y^+ - M_y^-}{\left(dM_y \big/ dx\right)\Big|_{M_y = 0}} \quad \text{and} \quad h_\varepsilon = \frac{\varepsilon_{xy}^+ - \varepsilon_{xy}^-}{\left(d\varepsilon_{xy} \big/ dx\right)\Big|_{\varepsilon_{xy} = 0}}, \tag{3.18}$$

where the superscript + and – correspond to the values of the field variable at $x = \pm\infty$. Note that l_ε and l_M are characteristic length scales associated with fixed material parameters, whereas h_M and h_ε are boundary thicknesses that are computed from a solution to the governing field equations.

The domain wall energy is given as

$$\gamma_{\text{wall}} = \int_{-\infty}^{\infty} \left[\psi - \psi\left(\infty\right)\right] dx\,. \tag{3.19}$$

For a *given* set of parameters characteristic of the properties of NiMnGa, Figures 1-3 indicate that the perfectly coupled theory gives rise to magnetic domain walls that are approximately one tenth the thickness of those in the general theory. Additionally, the twin boundary thickness for the perfectly coupled theory must be identical to the magnetic domain wall thickness, whereas the more general theory allows for arbitrary differences in these thicknesses. For the case shown in Figure 3, the magnetic domain wall thickness is approximately 3 times the twin boundary thickness. Finally, the domain wall energies predicted from the perfectly coupled theory are significantly higher than those from the general theory. To make this comparison, it is more informative to apply some representative values for the material coefficients and to scale the domain wall thicknesses such that they are equal lengths in both theories. Using the parameter values outlined in the Appendix and selecting the magnetic domain wall thickness for the 180º Bloch walls to be 20 nm, the domain wall energies predicted from each theory are given in Table 1.

	γ^{180}_{Bloch}	γ^{180}_{Neel}	γ^{90}_{twin}
Perfectly Coupled Theory	2220 mJ/m^2	1750 mJ/m^2	1040 mJ/m^2
General Theory	8 mJ/m^2	13 mJ/m^2	72 mJ/m^2

Table 1. Domain wall energies as predicted by the perfectly coupled and general theories assuming that the 180º Bloch walls in either theory are 20 nm thick.

Note that these are the energies associated with the simulations plotted in Figures 1-3. Also note that the $\boldsymbol{f}$ tensor was set to zero in the perfectly coupled theory. If this tensor were included, then the energies for the perfectly coupled theory would increase by about a factor of 5. We are not aware of any measurements of domain wall energies for NiMnGa, however magnetic domain walls in many magnetic materials are on the order of 10-20 nm thick and have domain wall energies in the 10-100 mJ/m^2 range. Hence, these computations suggest that the very strong elastic interaction associated with the perfectly coupled theory yields an unrealistic description of domain walls in ferromagnetic shape memory alloys. This fact, along with the feature that the more general theory allows for distinct domain wall and twin boundary length scales makes the general theory a more attractive option for modeling domain structure evolution in ferromagnetic shape memory allows.

Next, the general theory is applied to model the dissociation of a 90º domain wall from its coupled twin boundary. The appeal of FSMAs is the potential for relatively large actuation strains activated by remote magnetic fields. However, the primary drawback for these materials is the low blocking stress required to restrict any actuation displacement, Kiefer *et al*. (2007). In general, every active material has some finite blocking stress for a given actuating field. The method that we propose to investigate

this phenomenon is through the Eshebly driving traction on a 90º domain wall/twin boundary. Equation (3.11) indicates that if the driving traction on the coupled wall vanishes then the wall will not move. The large actuating strains that could be achieved by FSMAs can only occur through the motion of domain walls and hence the blocking stress can be determined from Equation (3.11) by setting the domain wall velocity to zero. Prior to making detailed calculations it is instructive to construct an approximation to Equation (3.11). For an infinite planar domain wall in the *y*-*z* plane loaded by a remote magnetic field in the *y*-direction H and a σ_{xy} component of shear stress τ, the driving force on the wall can be approximated as

$$f \approx \mu_0 \sqrt{2} M_s H + 3\varepsilon_0 \tau . \tag{3.20}$$

Here $\sqrt{2}M_s$ is the jump in the *y*-component of the magnetization across the domain wall, and $3\varepsilon_0$ is the jump in the engineering shear strain across the wall. Note that the constant ε_0 does carry a sign, and for NiMnGa is less than zero. This formula suggests an approximately linear relationship between the blocking stress and the applied magnetic field,

$$\tau_{block} \approx -\frac{\mu_0 \sqrt{2} M_s}{3\varepsilon_0} H . \tag{3.21}$$

In fact, this result is valid for the perfectly coupled model up to very large levels of H (for H nearly equal to the applied field required to cause homogeneous switching of the magnetization). This result is also valid for the general model at low levels of applied field. However, due to the independence of the magnetic domain wall from the twin boundary, there exists some level of applied shear stress such that no level of applied field, no matter how large, can cause actuation. The mechanism for this phenomenon is that the magnetic wall is driven in one direction *separately* from the twin boundary, which moves away in the opposite direction. We refer to this phenomenon as *domain wall/twin boundary dissociation*.

To elucidate this mechanism, consider only the equilibrium states of a coupled martensite twin boundary and magnetic domain wall. Furthermore, consider a loading state such that the applied magnetic field tends to move the magnetic wall to the right and the applied shear stress tends to move the twin boundary to the left. For relatively low load levels, if the shear stress is less than τ_{block} then no equilibrium state can be found and the magnetic wall and twin boundary move in concert to the right due to the dominating magnetic field. However, if the applied shear stress is greater than τ_{block},

then once again no equilibrium state can be found and the magnetic wall and twin boundary move together to the left due to the dominating shear stress. Equilibrium states of the domain wall can only be found when the applied sear stress is equal to τ_{block}. The calculations performed in this work investigate such states. For low levels of applied loading in the appropriate proportions, the magnetic wall tends to move to the right and the twin boundary tends to move to the left. However, due to the coupling between the walls this relative separation is limited, and an equilibrium configuration with zero wall velocities can be found. As the applied magneto-mechanical loading is increased, again in the appropriate proportions so as to maintain equilibrium, the relative separation between the magnetic wall and twin boundary increases. Eventually, a maximum is attained in the loading versus relative separation behavior, such that equilibrium states at higher load levels cannot be found. Above this maximum load level the magnetic wall moves off to the right and the twin boundary moves off to the left, which is what is referred to as domain wall/twin boundary dissociation. Detailed calculations of this behavior are presented next.

Figures 4a and 4b plot the "load-deflection" responses of the domain wall and twin boundary during the dissociation process for two different sets of material parameters. The load parameter F is given as

$$F = \sqrt{\frac{\sqrt{2}\mu_0 M_s^2}{3\sigma_0\left|\varepsilon_0\right|}}\frac{H}{M_s} = \sqrt{\frac{3\sigma_0\left|\varepsilon_0\right|}{\sqrt{2}\mu_0 M_s^2}}\frac{\tau}{\sigma_0}. \tag{3.22}$$

The deflection parameter δ is the distance between the point where the y-component of the magnetization is zero and the point where the shear component of the free strain is zero,

$$\delta = x\Big|_{M_y=0} - x\Big|_{\varepsilon^0_{xy}=0}. \tag{3.23}$$

Figures 4c and 4d illustrate the magnetization and shear strain profiles around the walls at the peak load levels for each case. Figures 4e and 4f are the magnetization and shear strain profiles after the walls are separated by significant distance, and the load-deflection behavior has reached a plateau.

There are several interesting features of the dissociation behavior. First, the load-deflection behavior has an initial linear regime indicating that there is a restoring force that brings the domain wall and twin boundary back together once they are separated by a small distance. The linear "stiffness" associated with this initial behavior will be characterized by the parameter k_w defined as

$$k_w = \frac{d\left(\tau_{block}/\sigma_0\right)}{d\left(\delta/l_\varepsilon\right)} \tag{3.24}$$

Additionally, for the behavior associated with the two sets of material properties shown here, there is a peak in the load-deflection response followed by a flat plateau region where the additional separation of the domain wall and twin boundary occurs at a relatively constant level of loading. We note that the existence of a peak in the load-deflection behavior is not universal. Qualitatively, a peak in the load deflection behavior occurs when the magnetic domain wall thickness, h_M, is longer than the martensite twin boundary thickness, h_ε. In such cases the peak *F* occurs at a level of δ close to h_M. On the other hand, when the magnetic domain wall is much thinner than the twin boundary, the peak disappears and the load-deflection behavior exhibits a smooth approach to the plateau level of *F*. In these cases, *F* is nearly at the plateau level when δ is on the order of h_ε. In contrast to the peak level of *F*, the plateau level in the load-deflection response is entirely independent of the boundary thicknesses, h_M and h_ε. This feature arises because the plateau level of *F* depends only on the states far from the walls where the field gradients vanish, while the peak level of *F* is due to the nonlinear interactions within the walls where the field gradients are highest.

The final sets of results appear in Figures 5a and 5b, and show the wall coupling stiffness k_w and the critical level of shear stress required to suppress any magnetic actuation, τ_c. These properties are displayed as functions of the relative magnetic wall thickness, h_M/h_ε, over a range of the other significant dimensionless material parameters, $\sigma_0\left|\varepsilon_0\right|/\mu_0 M_s^2$ and $K_1/\sigma_0\left|\varepsilon_0\right|$. Note that the quantities $b_1\left|\varepsilon_0\right|/\sigma_0$ and $b_4\left|\varepsilon_0\right|/\sigma_0$ have very small influences on the simulation results presented here. Figure 5a shows that the normalized wall stiffness $k_w\sigma_0\left|\varepsilon_0\right|/K_1$ as a function of h_M/h_ε at least approximately falls on a single universal curve for $0.25 < \sigma_0\left|\varepsilon_0\right|/\mu_0 M_s^2 < 25$ and $0.002 < K_1/\sigma_0\left|\varepsilon_0\right| < 0.4$. The dashed line that falls below this universal curve at high levels of h_M/h_ε represents the wall coupling stiffness for $K_1/\sigma_0\left|\varepsilon_0\right| = 0.8$ and $\sigma_0\left|\varepsilon_0\right|/\mu_0 M_s^2 = 2.5$, and this curve is rather insensitive to the $\sigma_0\left|\varepsilon_0\right|/\mu_0 M_s^2$ ratio. Therefore, for $K_1/\sigma_0\left|\varepsilon_0\right|$ greater than about 0.4 the universal curve is no longer valid at large magnetic domain wall thicknesses. For NiMnGa, $K_1 \approx 1\times10^5 - 2\times10^5$ J/m^3,

$\varepsilon_0 \approx -0.06$, and assuming that the characteristic stress is in the range $\sigma_0 \approx 100\,\text{MPa} - 10\,\text{GPa}$, the dimensionless anisotropy constant falls in the range $K_1/\sigma_0|\varepsilon_0| \approx 0.002 - 0.4$.

The critical blocking stress τ_c is of more significant interest. As previously discussed, for applied shear stress levels at or above τ_c, no level of applied magnetic field can cause coupled domain wall and twin boundary motion, which would lead to significant actuation strains. Instead, the magnetic domain wall and the martensite twin boundary dissociate as illustrated in Figure 4. Figure 5b plots the normalized critical blocking stress $\tau_c|\varepsilon_0|/K_1$ as a function of h_M/h_ε, for $\sigma_0|\varepsilon_0|/\mu_0 M_s^2$ = 0.25 and 2.5, and $K_1/\mu_0 M_s^2$ = 0.22 and 2.2. The new dimensionless parameter $K_1/\mu_0 M_s^2$ is simply a combination of the previous two, but it has been introduced because the normalized critical blocking stress is effectively independent of $\sigma_0|\varepsilon_0|/\mu_0 M_s^2$, and primarily a function of $K_1/\mu_0 M_s^2$. Furthermore, for large relative magnetic domain wall thicknesses, which we believe is the appropriate regime for NiMnGa, an upper plateau is reached for the blocking stress. Therefore, in the regime where $h_M > h_\varepsilon$, and using the specific magneto-mechanical coupling terms of lines 2-4 of Equation (2.36), the critical blocking stress predicted from this model is

$$\tau_c \approx K_1/2|\varepsilon_0|. \tag{3.25}$$

A second functional form for the magneto-mechanical coupling term has also been investigated by replacing lines 2-5 of Equation (2.36) with the following magnetocrystalline anisotropy energy,

$$\begin{aligned}\psi_K = {} & \frac{2K_1}{3\varepsilon_0^2 M_s^2}\left[\left(\varepsilon_{11}^0 + \varepsilon_0/2\right)^2\left(M_2^2 + M_3^2\right) + \left(\varepsilon_{22}^0 + \varepsilon_0/2\right)^2\left(M_1^2 + M_3^2\right) + \left(\varepsilon_{33}^0 + \varepsilon_0/2\right)^2\left(M_1^2 + M_2^2\right)\right] \\ & + \frac{K_2}{\varepsilon_0 M_s^2}\left[\left(\varepsilon_{12}^0 + \varepsilon_{21}^0\right)M_1 M_2 + \left(\varepsilon_{13}^0 + \varepsilon_{31}^0\right)M_1 M_3 + \left(\varepsilon_{23}^0 + \varepsilon_{32}^0\right)M_2 M_3\right]\end{aligned} \tag{3.26}$$

Note that both forms of the magnetocrystalline anisotropy energy yield the same slope for the mechanically-clamped hard-axis magnetization curve, $dM/dH = \mu_0 M_s^2/3K_1$. For either of these two magntocrystalline anisotropy energies, the calculations show that the same qualitative and very nearly the same quantitative behaviors appear for Figures 5a and 5b, such that the level of the upper plateau for the critical blocking stress

remains at $\tau_c \left|\varepsilon_0\right| / K_1 \approx 0.5$. Therefore, if we again consider the properties of NiMnGa, the critical blocking stress predicted by this theory for NiMnGa is $\tau_c \approx 1-2$ MPa, corresponding to a compressive stress of about 2-4 MPa, which is in the range of 2-6 MPa reported by recent measurements, Karaca *et al*. (2006) and Kiefer *et al*. (2007).

4. Discussion

In this work a theory to describe the magnetic domain and martensite twin structure evolution in ferromagnetic shape memory alloys is described. A new approach for the derivation of the fundamental equations governing the behavior of the magnetization and the martensite free strain is presented. The key idea is to postulate the existence of generalized micro-forces that do work as the order parameters, i.e. magnetization and free strain, change. Overall balances of these micro-forces are then established taking the same physical footing as mechanical equilibrium and Gauss' law within the theory. It is demonstrated, by applying established continuum methods for analyzing the consequences of the second law of thermodynamics, that the micro-force balances ultimately lead to the commonly accepted Landau-Lifshitz-Gilbert evolution equations of micromagnetics for the magnetization, and a time-dependent Landau-Ginzburg type evolution equation for the martensite free strain. We note that the uncoupled version of the theory applies to standard ferromagnetic materials and shape memory alloys if the magneto-mechanical coupling does not exist.

The theoretical framework is applied to investigate the fields near domain walls and twin boundaries in FSMAs. First, some general analytic results are presented for walls moving at constant velocity, and a kinetic relationship between the wall velocity and the driving force on the wall (the jump in the Eshelby energy-momentum tensor) is derived. Numerical simulations show that a theory that rigidly couples the martensite strain to the magnetization, as is done for ferroelectrics, leads to either unrealistically thin or very high-energy domain walls. Based on this result it is ascertained that the general, more weakly coupled theory is more appropriate for describing domain walls and twin boundaries in FSMAs. The general theory is able to predict the unfortunately low critical levels of blocking stress in FSMAs.

It is postulated that the dissociation of 90° magnetic domain walls and the martensite twin boundaries is the mechanism responsible for the low critical blocking stress in FSMAs. This mechanism is studied within numerical simulations where combined states of shear stress and magnetic field are applied to the material such that the domain wall/twin boundary system remains stationary. At low levels of combined loading the walls remain connected with their separation governed by an elastic type of behavior. As the combined loading is increased, a peak is eventually reached such that

the magnetic domain wall and the martensite twin boundary move in opposite directions. The implication from this behavior is that if the applied stress is higher than this peak, then no level of applied magnetic field is able to drive coupled domain wall/twin boundary motion, and hence no significant actuating strain can be produced. The theory places the critical compressive blocking stress for NiMnGa in the range of 2-4 MPa, which is in agreement with experimental observations.

Acknowledgement

The author would like to acknowledge support from the National Science Foundation under project number CMMI-0719071.

References

Brown, W.F. 1963. *Micromagnetics*. John Wiley & Sons, New York, USA.

Chen, L.Q., 2002. Phase-field models for microstructure evolution. *Annual Review of Materials Research* 32, 113-140.

Coleman, R.D. and Noll, W. 1963. The thermodynamics of elastic materials with heat conduction and viscosity. *Archive of Rational Mechanics and Analysis* 13, 167-178.

Dai, L., Cullen, J. and Wuttig, M. 2004. Intermartensitic transformation in a NiMnGa alloy. *Journal of Applied Physics* 95, 6957-6959.

DeSimone, A. and James, R.D. 1997. A theory of magnetostriction oriented to-wards applications. *Journal of Applied Physics* 81, 5706-5708.

DeSimone, A. and James, R.D. 2002. A constrained theory of magnetoelasticity. *Journal of the Mechanics and Physics of Solids* 50, 283-320.

DeSimone, A., Kohn, R.V., Müller, S. and Otto, F., 2006. Recent analytical developments in micromagnetics, in The Science of Hysteresis II: Physical Modeling, Micromagnetics, and Magnetization Dynamics, G, Berotti and I. Mayergoyz eds. pp. 269-381, Elsevier.

Eshelby, J.D., 1970. Energy relations and the energy-momentum tensor in continuum mechanics. *Inelastic Behavior of Solids*, 77-115.

Fried, E. and Gurtin, M.E. 1993. Continuum theory of thermally induced phase transitions based on an order parameter. *Physica D* 68, 326-343.

Fried, E. and Gurtin, M.E. 1994. Dynamic solid-solid transitions with phase characterized by an order parameter. *Physica D* 72, 287-308.

Gilbert, T.L. 1956. *Formulation, Foundations, and Applications of the Phenomenological Theory of Ferromagnetism.* PhD Thesis. Illinois Institute of Technology.

Gilbert, T.L. 2004. A phenomenological theory of damping in ferromagnetic materials. *IEEE Transactions on Magnetics* 40, 3443-3449.

Givoli, D. and Keller, J.B. 1989. A finite-element method for large domains. *Computer Methods in Applied Mechanics and Engineering* 76, 41-66.

Gurtin, M.E. 1996. Generalized Ginzburg-Landau and Cahn-Hilliard equations based on a microforce balance. *Physica D* 92, 178-192.

Gurtin, M.E., Weissmüller, J. and Larché, F. 1998. A general theory for curved deformable interfaces in solids at equilibrium. *Philosophical Magazine A* 78, 1093-1109.

James, R.D. and Wuttig, M. 1998. Magnetostriction of martenstite. *Philosophical Magazine A* 77, 1273-1299.

Jin, Y.M., Artemev, A. and Khachaturyan, A.G. 2001. Three-dimensional phase field model of low-symmetry martensitic transformation in polycrystal: simulation of ζ'_2 martensite in AuCd alloys. *Acta Materialia* 49, 2309-2320.

Karaca, H.E., Karaman, I., Basaran, B., Chumlyakov, Y.I. and Maier, H.J. 2006. Magnetic field and stress induced martensite reorientation in NiMnGa ferromagnetic shape memory alloy single crystals. *Acta Materialia* 54, 233-245.

Kiefer, B. and Lagoudas, D.C. 2005. Magnetic field-induced martensitic reorientation in magnetic shape memory alloys. *Philosophical Magazine* 85, 4289-4329.

Kiefer, B., Karaca, H.E., Lagoudas, D.C. and Karaman, I. 2007. Characterization and modeling of the magnetic field-induced strain and work output in magnetic shape memory alloys. *Journal of Magnetism and Magnetic Materials* 312, 164-175.

Kronmüller, H. and Fähnle, M., 2003. *Micromagnetism and the Microstructure of Ferromagnetic Solids*. Cambridge University Press.

Landau, L.D. and Lifsitz, E.M. 1935. On the theory of the dispersion of magnetic permeability in ferromagnetic bodies. *Phys. Z. Sowjet* 8 153-169.

Ma, Y.F. and Li, J.Y. 2007a. A constrained theory on actuation strain in ferro-magnetic shape memory alloys induced by domain switching. *Acta Materialia* 55, 3261-3269.

Ma, Y.F. and Li, J.Y. 2007b. Magnetization rotation and rearrangement of martensite variants in ferromagnetic shape memory alloys. *Applied Physics Letters* 90, 172504.

Murray, S.J., Marioni, M., Tello, P.G., Allen, S.M. and O'Handley, R.C., 2001. Giant magnetic-filed-induced strain in Ni-Mn-Ga crystals: experimental results and modeling. *Journal of Magnetism and Magnetic Materials* 226-230, 945-947.

Nye, J.F. 1957. *Physical properties of crystals*. Oxford University Press, Great Britain.

O'Handley, R.C., Murray, S.J., Marioni, M., Nembach, H. and Allen, S.M. 2000. Phenomenology of giant magnetic-field-induced strain in ferromagnetic shape-memory alloys. *Journal of Applied Physics* 87, 4712-4717.

Sozinov, A., Likhachev, A.A., Lanska, N. and Ullakko, K., 2002. Giant magnetic-field-induced strain in NiMnGa seven-layered martensitic phase. *Applied Physics Letters* 80, 1746-1748.

Su, Y. and Landis, C.M., 2007. Continuum thermodynamics of ferroelectric domain evolution: theory, finite element implementation, and application to domain wall pinning. *Journal of the Mechanics and Physics of Solids* 55, 280-305.

Thiele, A.A., 1974. Applications of the gyrocoupling vector and dissipation dyadic in the dynamics of magnetic domains. *Journal of Applied Physics* 45, 377-393.

Tickle, R. and James, R.D., 1999. Magnetic and magnetomechanical properties of Ni_2MnGa. *Journal of Magnetism and Magnetic Materials* 195 627-638.

Tickle, R. 2000. *Ferromagnetic Shape Memory Materials*. PhD Thesis. University of Minnesota.

Wang, Y.U., Jin, Y.M. and Khachaturyan, A.G. 2004. The effects of free surfaces on martensite microstructures: 3D phase field microelasticity simulation study. *Acta Materialia* 52, 1039-1050.

Zhang, J.X. and Chen, L.Q. 2005a. Phase-field model for ferromagnetic shape-memory alloys. *Philosophical Magazine Letters* 85, 533-541.

Zhang, J.X. and Chen, L.Q. 2005b. Phase-field microelasticity theory and micromagnetic simulations of domain structures in giant magnetostrictive materials. *Acta Materialia* 53, 2845-2855.

Appendix

The specific form for the Helmholtz free energy applied in this work is given in Equation (2.36) and is repeated below. In a coordinate system with the Cartesian axes aligned with the ⟨100⟩ directions, this form of the free energy that can be used to mimic the properties of single crystals with a tetragonal martensite phase and an easy magnetization axis aligned with the *c*-axis of the unit cell.

$$\begin{aligned}
\psi = {} & \tfrac{1}{2}a_0^M M_{i,j}M_{i,j} + \tfrac{1}{2}a_0^\varepsilon \varepsilon_{ij,k}^0 \varepsilon_{ij,k}^0 \\
& + \frac{K_1}{\varepsilon_0 M_s^2}\left[\left(\varepsilon_{11}^0 + \varepsilon_0/2\right)\left(M_2^2 + M_3^2\right) + \left(\varepsilon_{22}^0 + \varepsilon_0/2\right)\left(M_1^2 + M_3^2\right) + \left(\varepsilon_{33}^0 + \varepsilon_0/2\right)\left(M_1^2 + M_2^2\right)\right] \\
& - \frac{2}{3}\frac{K_1}{\varepsilon_0^2}\left[\varepsilon_{11}^0\varepsilon_{22}^0 + \varepsilon_{11}^0\varepsilon_{33}^0 + \varepsilon_{22}^0\varepsilon_{33}^0 + \varepsilon_0\left(\varepsilon_{11}^0 + \varepsilon_{22}^0 + \varepsilon_{33}^0\right)\right] \\
& + \frac{K_2}{\varepsilon_0 M_s^2}\left[\left(\varepsilon_{12}^0 + \varepsilon_{21}^0\right)M_1M_2 + \left(\varepsilon_{13}^0 + \varepsilon_{31}^0\right)M_1M_3 + \left(\varepsilon_{23}^0 + \varepsilon_{32}^0\right)M_2M_3\right] \\
& + \frac{b_1}{2}\left(\varepsilon_{kk}^0\right)^2 + \frac{b_2}{3}\left[\left(e_{11}^0\right)^3 + \left(e_{22}^0\right)^3 + \left(e_{33}^0\right)^3\right] + \frac{b_3}{4}\left[\left(e_{11}^0\right)^4 + \left(e_{22}^0\right)^4 + \left(e_{33}^0\right)^4\right] \\
& + \frac{b_4}{2}\left[\left(\varepsilon_{12}^0\right)^2 + \left(\varepsilon_{21}^0\right)^2 + \left(\varepsilon_{13}^0\right)^2 + \left(\varepsilon_{31}^0\right)^2 + \left(\varepsilon_{23}^0\right)^2 + \left(\varepsilon_{32}^0\right)^2\right] \\
& + \tfrac{1}{2}\bar{c}_{ijkl}\left(\varepsilon_{ij} - \varepsilon_{ij}^0\right)\left(\varepsilon_{kl} - \varepsilon_{kl}^0\right) \\
& + \frac{1}{2\mu_0}B_iB_i - M_iB_i + \frac{\mu_0\left(1+\chi_m\right)}{2\chi_m}\left(M - M_s\right)^2 + \mu_0 M_s M
\end{aligned} \tag{A.1}$$

$$e_{ij}^0 = \varepsilon_{ij}^0 - \tfrac{1}{3}\varepsilon_{kk}^0\delta_{ij} \text{ and } M = \sqrt{M_iM_i} \tag{A.2}$$

For our calculations we have chosen values for these parameters that mimic NiMnGa. It is useful to express these parameters in dimensionless form. To do this we introduce a characteristic stress, σ_0, such that the height of the energy barrier given by the *b*-terms is $\sigma_0\varepsilon_0$. This then implies that,

$$b_2 = -16\frac{\sigma_0\varepsilon_0}{\left|\varepsilon_0^3\right|} \text{ and } b_3 = \frac{32}{3}\frac{\sigma_0}{\left|\varepsilon_0^3\right|} \tag{A.3}$$

For a martensite variant with its c-axis oriented in the x_1 direction, the curvature components of the energy wells defined by Equation (2.41) are then,

$$f_{1111} = b_1 + \frac{16}{3}\frac{\sigma_0}{|\varepsilon_0|}, \quad f_{2222} = f_{3333} = b_1 + \frac{40}{3}\frac{\sigma_0}{|\varepsilon_0|},$$
$$f_{1122} = f_{1133} = b_1 - \frac{8}{3}\frac{\sigma_0}{|\varepsilon_0|}, \quad f_{2233} = b_1 - \frac{32}{3}\frac{\sigma_0}{|\varepsilon_0|} \tag{A.4}$$

The characteristic values for NiMnGa are, $M_s = 6\times10^5$ A/m, $\varepsilon_0 = -0.06$, $\sigma_0 = 200$ MPa, $b_1 = 40\sigma_0/|\varepsilon_0|$, $b_4 = 30\sigma_0/|\varepsilon_0|$, $K_1 = K_2 = 1\times10^5 - 2\times10^5$ J/m^3, $\mu_0 = 4\pi\times10^{-7}$ N/A^2, $\chi_m = 10^{-5}$, and the principal values of $\bar{c}_{ijkl}$ are $10^5\sigma_0/|\varepsilon_0|$. The parameter ranges that have been investigated in this paper surround these values. These choices for the parameters lead to elastic properties very similar to those measured by Dai *et al*. (2004), and yield a slope for the hard-axis, mechanically clamped *M-H* curve of $dM/dH = \mu_0 M_s^2/3K_1$. The choices for a_M^0 and a_ε^0 simply set the length scales within the problem as defined by Equations (3.16) and (3.17).

Figure Captions

Figure 1. The magnetization and stress distributions near a 180º Bloch wall (magnetization rotates in the *y*-*z* plane). The arrows in the small inset figure nominally represent the magnetization on either side of the domain wall located at $x = 0$. (a)-(b) The magnetization and stress distributions for the reduced/constrained theory. (c)-(d) The corresponding distributions for the general theory allowing for distinct magnetic domain walls and martensite twin boundaries.

Figure 2. The magnetization and stress distributions near a 180º Néel wall (magnetization rotates in the *x*-*y* plane). The arrows in the small inset figure nominally represent the magnetization on either side of the domain wall located at $x = 0$. (a)-(b) The magnetization and stress distributions for the reduced/constrained theory. (c)-(d) The corresponding distributions for the general theory allowing for distinct magnetic domain walls and martensite twin boundaries.

Figure 3. The magnetization and shear strain and stress distributions near a 90º magnetic domain wall/martensite twin boundary (magnetization rotates in the *x*-*y* plane). The arrows in the small inset figure nominally represent the magnetization on either side of the domain wall located at $x = 0$. (a)-(b) The magnetization and shear strain and stress distributions for the reduced/constrained theory. (c)-(d) The corresponding distributions for the general theory allowing for distinct magnetic domain walls and martensite twin boundaries.

Figure 4. The predicted magnetic domain wall/martensite twin boundary dissociation process in ferromagnetic shape memory alloys. The normalized material properties for these simulation are shown on (a) and (b). Plots (c) and (e) correspond to (a), and (d) and (f) correspond to (b). (a)-(b) The load F – deflection δ behavior for the domain wall/twin boundary, quasi-statically loaded by simultaneous shear stress and magnetic field such that the walls have zero velocity. F is defined in Equation (3.22) and δ is defined in Equation (3.23). (c)-(d) The magnetization and shear strain profiles at the peak of the load-deflection behavior. (e)-(f) The magnetization and shear strain profiles once the domain wall and twin boundary are separated by a significant distance.

Figure 5. (a) The normalized initial slope of the F-δ behavior as a function of the relative domain wall to twin boundary thickness. The parameter k_w is defined in Equation (3.24). This parameter is relatively insensitive to both the $\sigma_0 \left|\varepsilon_0\right| \Big/ \mu_0 M_s^2$ and $K_1 \Big/ \sigma_0 \left|\varepsilon_0\right|$ ratios for $K_1 \Big/ \sigma_0 \left|\varepsilon_0\right| < 0.4$. (b) The normalized critical level of applied

shear stress to suppress magnetically driven actuation strains. This shear stress level corresponds to the peak in the F-δ behavior. This behavior is relatively insensitive to the $\sigma_0 |\varepsilon_0| / \mu_0 M_s^2$ ratio for all values of h_M / h_ε, and insensitive to $K_1 / \mu_0 M_s^2$ and h_M / h_ε for large values of h_M / h_ε.

Figure 1

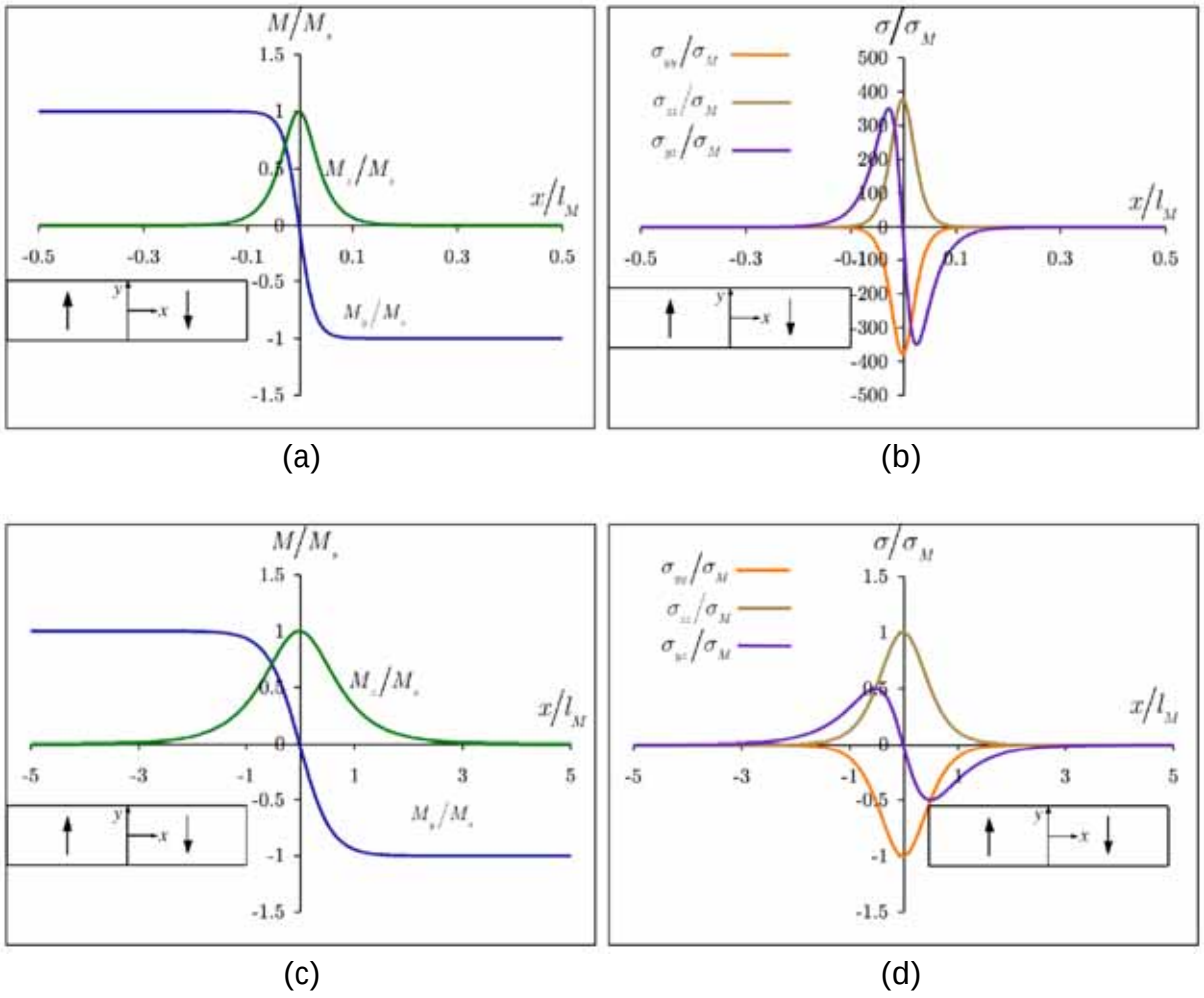

(a) (b)

(c) (d)

Figure 2

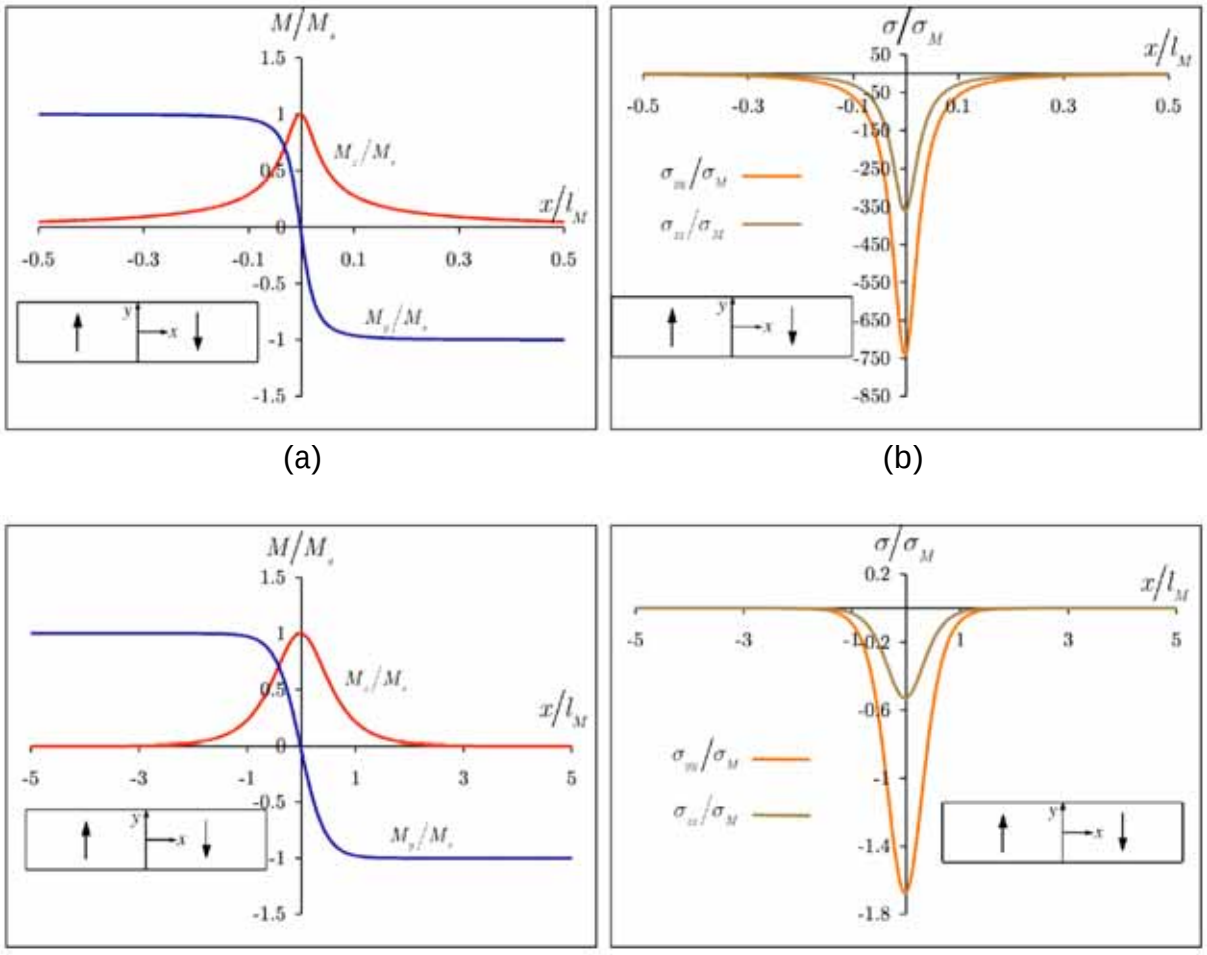

(a) (b)

(c) (d)

Figure 3

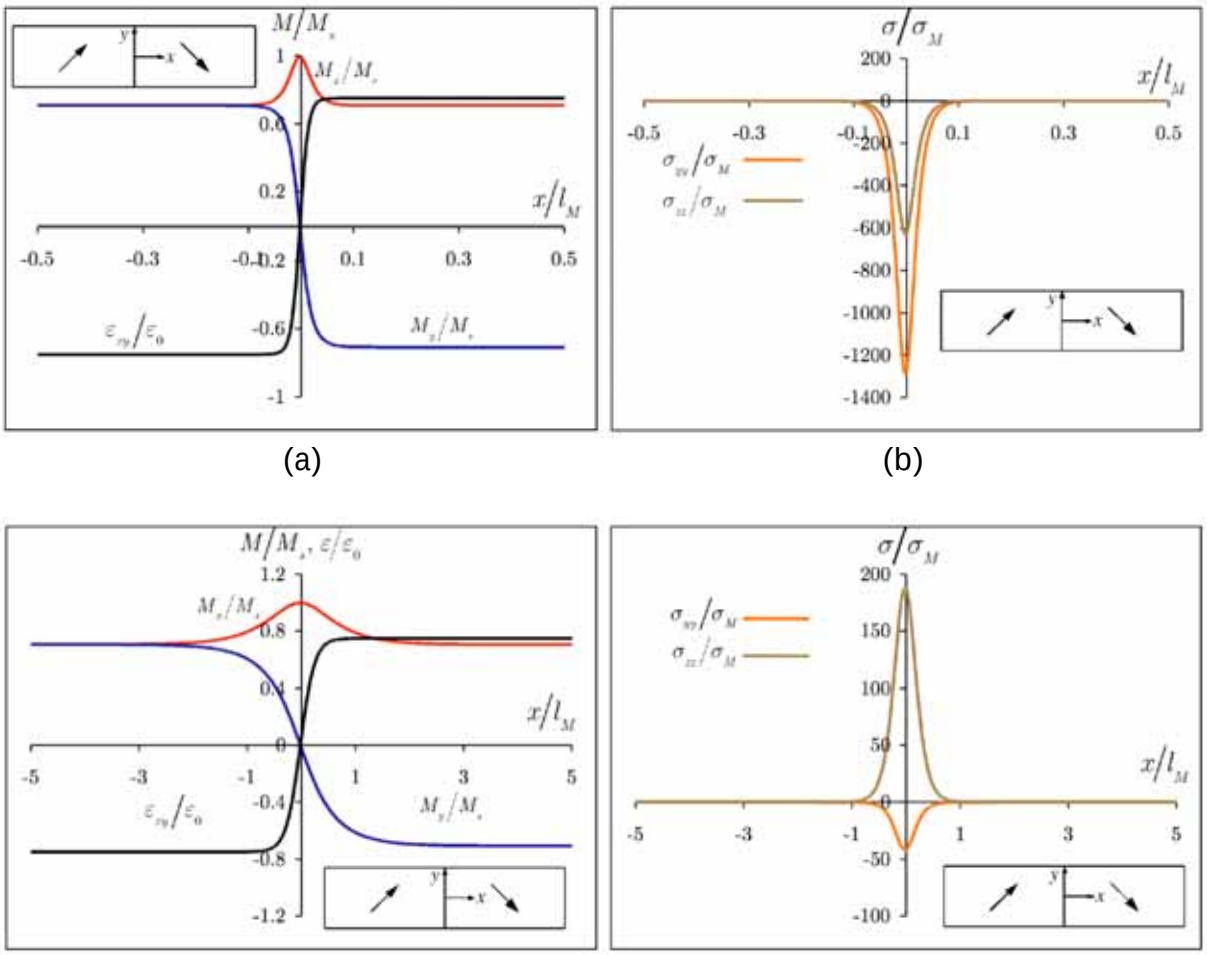

(a) (b)

(c) (d)

Figure 4

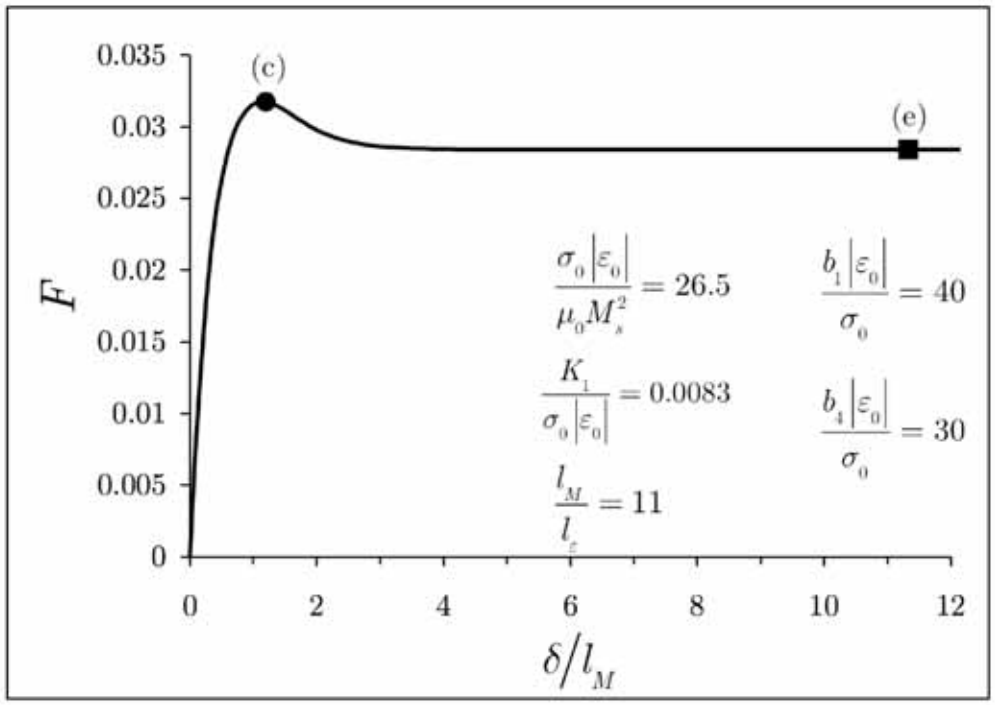
0.035
0.03
0.025
0.02
0.015
0.01
0.005
0
F
(c)
(e)
$\frac{\sigma_0|\varepsilon_0|}{\mu_0 M_s^2} = 26.5$
$\frac{b_1|\varepsilon_0|}{\sigma_0} = 40$
$\frac{K_1}{\sigma_0|\varepsilon_0|} = 0.0083$
$\frac{b_4|\varepsilon_0|}{\sigma_0} = 30$
$\frac{l_M}{l_c} = 11$
0
2
4
6
8
10
12
δ/l_M

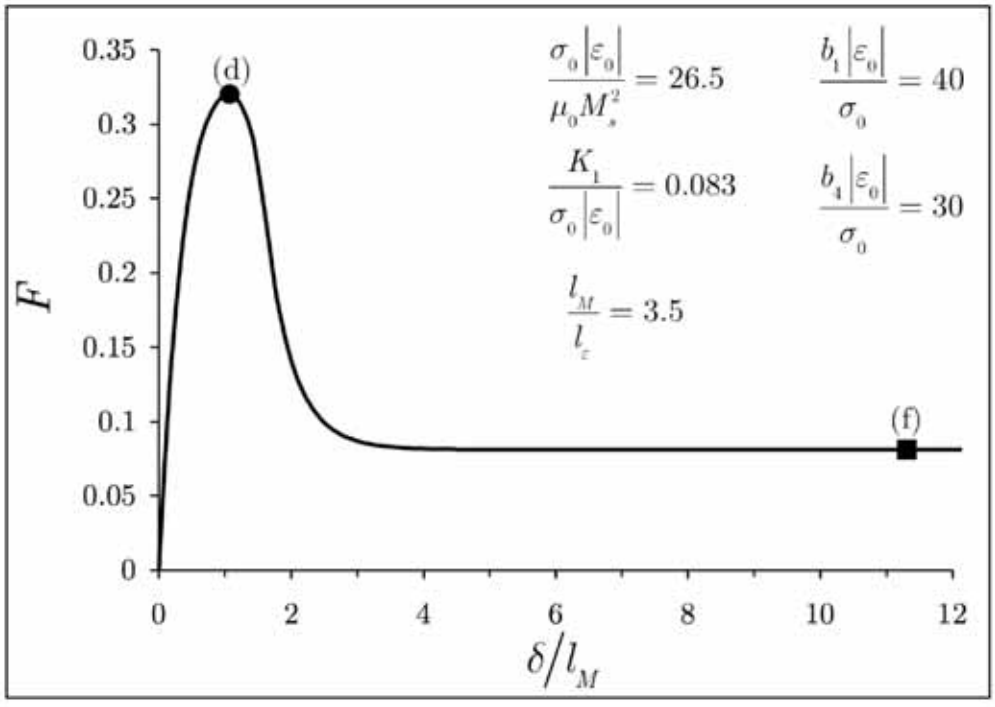
0.35
0.3
0.25
0.2
0.15
0.1
0.05
0
F
(d)
(f)
$\frac{\sigma_0|\varepsilon_0|}{\mu_0 M_s^2} = 26.5$
$\frac{b_1|\varepsilon_0|}{\sigma_0} = 40$
$\frac{K_1}{\sigma_0|\varepsilon_0|} = 0.083$
$\frac{b_4|\varepsilon_0|}{\sigma_0} = 30$
$\frac{l_M}{l_c} = 3.5$
0
2
4
6
8
10
12
δ/l_M

(a) (b)

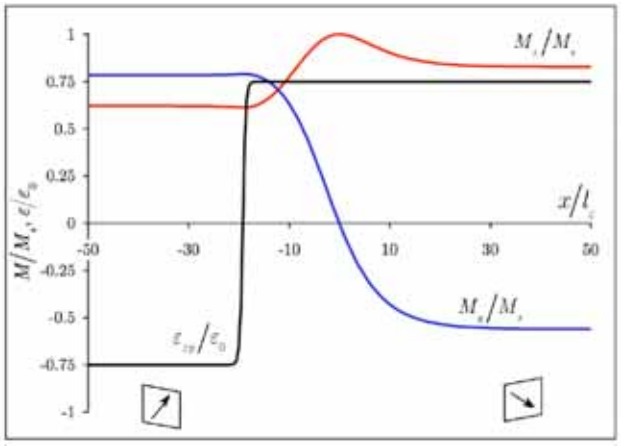
1
0.75
0.5
0.25
0
-0.25
-0.5
-0.75
-1
-50
-30
-10
10
30
50
M_x/M_s
x/l_c
M_z/M_s
$\varepsilon_{xy}/\varepsilon_0$
$M/M_s, \varepsilon/\varepsilon_0$

(c)

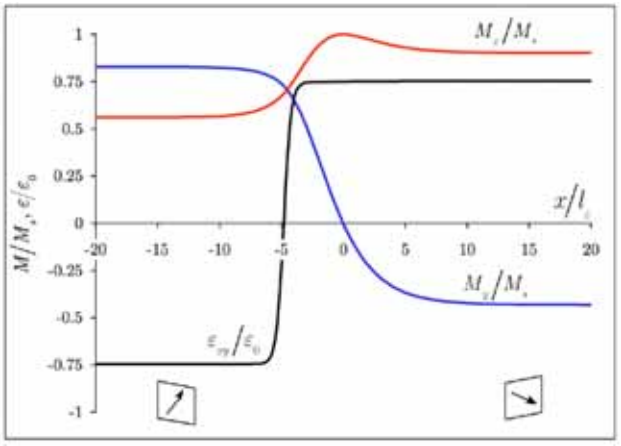
1
0.75
0.5
0.25
0
-0.25
-0.5
-0.75
-1
-20
-15
-10
-5
0
5
10
15
20
M_x/M_s
x/l_c
M_z/M_s
$\varepsilon_{xy}/\varepsilon_0$
$M/M_s, \varepsilon/\varepsilon_0$

(d)

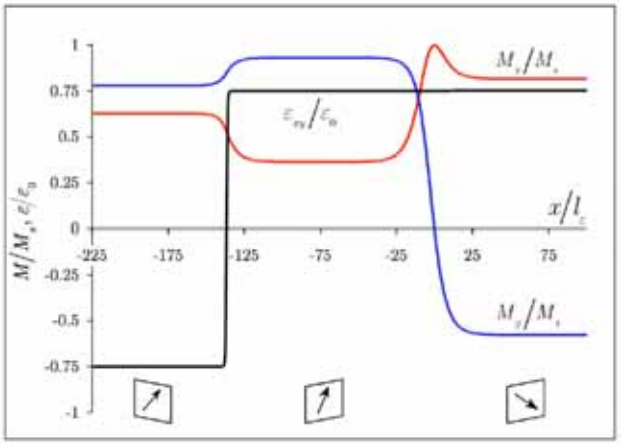
1
0.75
0.5
0.25
0
-0.25
-0.5
-0.75
-1
-225
-175
-125
-75
-25
25
75
M_x/M_s
$\varepsilon_{xy}/\varepsilon_0$
x/l_c
M_z/M_s
$M/M_s, \varepsilon/\varepsilon_0$

(e)

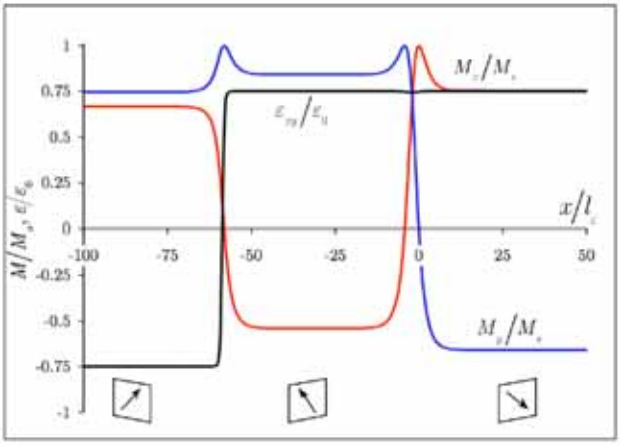
1
0.75
0.5
0.25
0
-0.25
-0.5
-0.75
-1
-100
-75
-50
-25
0
25
50
M_x/M_s
$\varepsilon_{xy}/\varepsilon_0$
x/l_c
M_z/M_s
$M/M_s, \varepsilon/\varepsilon_0$

(f)

Figure 5

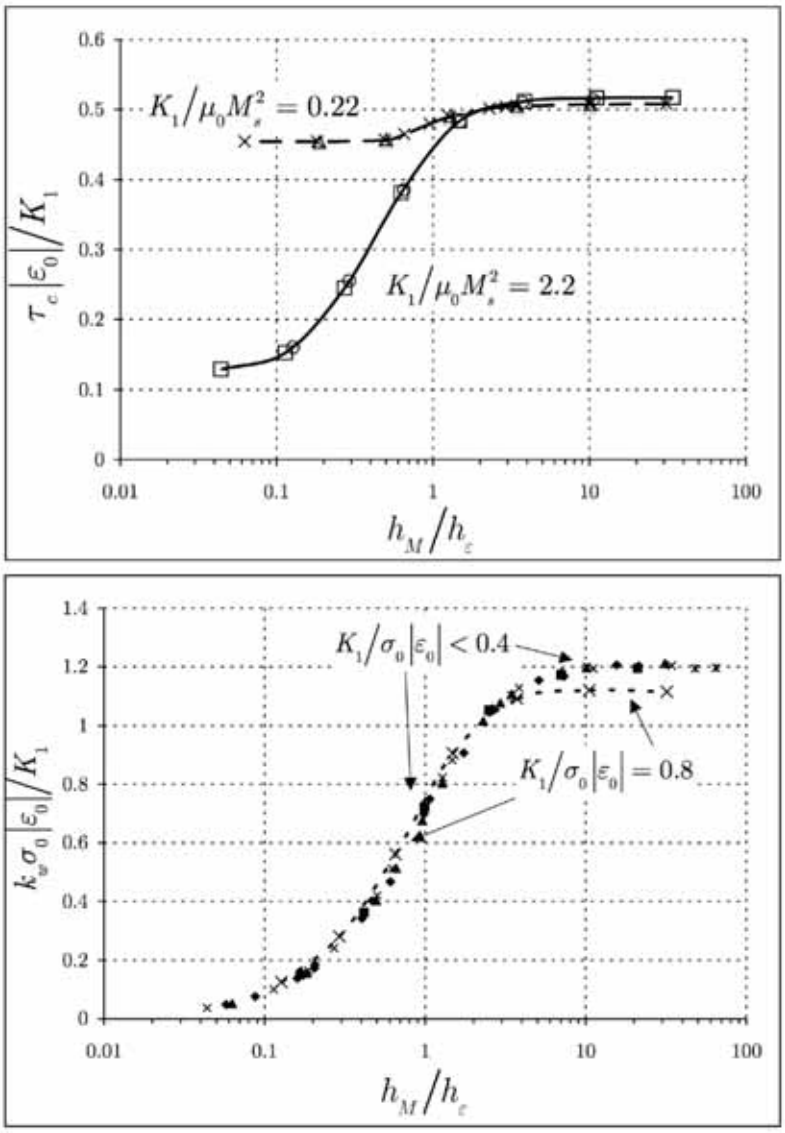
$K_1/\mu_0 M_s^2 = 0.22$
$K_1/\mu_0 M_s^2 = 2.2$
$\tau_c|\varepsilon_0|/K_1$
h_M/h_c
$K_1/\sigma_0|\varepsilon_0| < 0.4$
$K_1/\sigma_0|\varepsilon_0| = 0.8$
$k_w\sigma_0|\varepsilon_0|/K_1$
h_M/h_c